Palaeoseismology of the North Anatolian Fault near the Marmara Sea: implications for fault segmentation and seismic hazard

THOMAS ROCKWELL[1]*, DANIEL RAGONA[1], GORDON SEITZ[1], ROB LANGRIDGE[2], M. ERSEN AKSOY[3], GÜLSEN UCARKUS[3], MATTHIEU FERRY[4,7], ARON J. MELTZNER[5], YANN KLINGER[6], MUSTAPHA MEGHRAOUI[7], DILEK SATIR[3], AYKUT BARKA[3†] & BURCAK AKBALIK[3]

[1]*Geological Sciences, San Diego State University, San Diego, CA 92182, USA*

[2]*Institute of Geological and Nuclear Sciences, PO Box 30-368, Lower Hutt, New Zealand*

[3]*Eurasia Institute of Earth Sciences, Istanbul Technical University, Maslak, Istanbul, Turkey*

[4]*Universidade de Évora, Centro de Geofisica de Évora, Rua Romão Ramalho 59, 7002-554 Évora, Portugal*

[5]*Tectonics Observatory, California Institute of Technology, Pasadena, CA 91125, USA*

[6]*Laboratoire de Tectonique, Institut de Physique du Globe, 4 place Jussieu, 75005, Paris, France*

[7]*Institut de Physique de Globe, 5 rue René Descartes, F-67084 Strasbourg Cedex, France*

[†]*Deceased*

*Corresponding author (e-mail: Trockwel@geology.sdsu.edu)

Abstract: We conducted palaeoseismic studies along the North Anatolian fault both east and west of the Marmara Sea to evaluate its recent surface rupture history in relation to the well-documented historical record of earthquakes in the region, and to assess the hazard of this major fault to the city of Istanbul, one of the largest cities in the Middle East. Across the 1912 rupture of the Ganos strand of the North Anatolian fault west of the Marmara Sea, we excavated 26 trenches to resolve slip and constrain the earthquake history on a channel–fan complex that crosses the fault at a high angle. A distinctive, well-sorted fine sand channel that served as a marker unit was exposed in 21 trenches totaling over 300 m in length. Isopach mapping shows that the sand is channelized north of the fault, and flowed as an overflow fan complex across a broad fault scarp to the south. Realignment of the feeder channel thalweg to the fan apex required about 9 ± 1 m of reconstruction. Study of the rupture history in several exposures demonstrates that this displacement occurred as two large events. Analysis of radiocarbon dates places the age of the sand channel as post AD 1655, so we attribute the two surface ruptures to the large regional earthquakes of 1766 and 1912. If each was similar in size, then about 4–5 m of slip can be attributed to each event, consistent with that reported for 1912 farther east. We also found evidence for two additional surface ruptures after about AD 900, which probably correspond to the large regional earthquakes of 1063 and 1344 (or 1354). These observations suggest fairly periodic occurrence of large earthquakes ($RI = c. 283 \pm 113$ years) for the past millennium, and a rate of $c.$ 16 mm/a if all events experienced similar slip.

We excavated six trenches at two sites along the 1999 Izmit rupture to study the past earthquake history along that segment of the North Anatolian fault. One site, located in the township of Köseköy east of Izmit, revealed evidence for three surface ruptures (including 1999) during the past 400 years. The other trench was sited in an Ottoman canal that was excavated (but never completed) in 1591. There is evidence for three large surface rupturing events in the upper 2 m of alluvial fill within the canal at that site, located only a few kilometres from the Köseköy site. One of the past events is almost certainly the large earthquake of 1719, for which historical descriptions of damage are nearly identical to that of 1999. Other earthquakes that could plausibly be attributed to the other recognized rupture of the Izmit segment are the 1754, 1878 or 1894 events, all of which produced damage in the region and for which the source faults are poorly known. Our palaeoseismic observations suggest that the Izmit segment of the North Anatolia fault ruptures every one and a half centuries or so, consistent with the historical record for the region, although the time between ruptures may be as short as 35 years if 1754 broke the Izmit segment.

Release of about 4 m of seismic slip both west and east of the Marmara Sea this past century (1912, 1999) support the contention that Istanbul is at high risk from a pending large earthquake.

In that historical records suggest that the last large central Marmara Sea event occurred in 1766, there may be a similar 4 m of accumulated strain across the Marmara basin segment of the North Anatolian fault.

Information on the size and timing of past earthquakes is important in understanding fault behaviour, a key element in forecasting future seismic activity (Sieh 1996). The North Anatolian fault (NAF) in Turkey (Barka 1992) (Fig. 1) is an ideal candidate for understanding fault behaviour over multiple earthquake cycles because there is a long and excellent historical record of large earthquakes going back over 2000 years (Ambraseys & Finkel 1987*a*, *b*, 1991, 1995; Ambraseys 2002*a*, *b*). Furthermore, like the San Andreas fault of southern California, it is a fast-moving fault (*c.* 24 mm/a; Straub & Kahle 1995; Straub 1996; Reilinger *et al.* 1997; McClusky *et al.* 2000) resulting in many earthquakes during this long historical period. It is also segmented, and nearly all of the segments have ruptured this past century. Thus, there is the opportunity to collect information on the patterns of large earthquake ruptures and their sizes over several earthquake cycles. In this paper, we present new results that further quantify the earthquake history of the NAF both east and west of the Marmara Sea, and discuss their bearing on the seismic hazard to Istanbul.

To the west, near the Gulf of Saros, we extended our earlier palaeoseismic investigations along the Ganos strand and resolved slip for the past two large earthquakes that struck the Gallipoli region in 1766 and 1912. The Saros study area lies within the township of Kavakköy, close to where we completed earlier studies (Rockwell *et al.* 2001). We had determined that four surface ruptures occurred near where the fault passes offshore into the Gulf of Saros during the past 1100 years or so. However, the dating was insufficiently precise to confidently resolve which of the historical events these were. In this new study, we focused on a young (post AD 1655) stream channel that crosses the fault at a high angle and is offset by the fault across a narrow zone. Twenty-six trenches were excavated at this new site to resolve total slip on the channel and to further constrain the timing of ruptures that produced the slip.

East of the Marmara Sea, we continued efforts between Izmit and Lake Sapanca that we had begun prior to the August 1999 Izmit earthquake. Specifically, we excavated new trenches within and adjacent to an Ottoman canal, dated at *c.* 1591 from historical data (Finkel & Barka 1997; C. Finkel, pers. comm.) to resolve the history of surface ruptures for the past 400 years east of Izmit Bay.

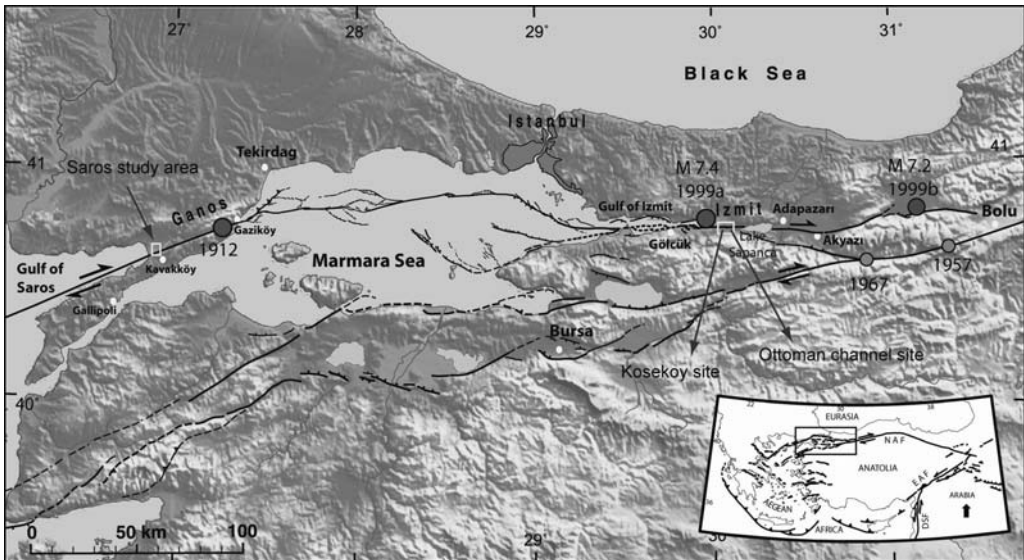Each of these studies bears on the impending seismic hazard to Istanbul, which lies close to

Fig. 1. Generalized map of active faults in NW Turkey, with recent large earthquakes. Note the three areas for this study relative to the Marmara Sea and Istanbul.

the NAF. Our observations support the contention that the NAF near Istanbul should be close to failure based on the distribution and size of earthquakes during the past 400 years, and that the recent earthquakes to the east (Izmit and Düzce events in 1999) have further loaded the fault segments beneath the Marmara Sea (Parsons *et al.* 2000).

The Saros site

Earlier palaeoseismic results at Kavakköy in the Gallipoli Peninsular region near the Gulf of Saros indicate that four earthquakes have ruptured the surface in that area during the past 1000–1200 years, and that two of these post-date a sand channel dated to younger than the fourteenth century AD (Rockwell *et al.* 2001). One of these is almost certainly the surface rupture of the 1912

M7.3 earthquake (Ambraseys 2002*a*), which was photographed east of our site towards Gaziköy (Ambraseys & Finkel 1987*a*) and has been studied in detail by Altunel *et al.* (2004).

We analysed low-altitude stereo photography of the fault along the westernmost few kilometres before it passes offshore into the Gulf of Saros (Fig. 2), to search for the best sites to resolve slip. In the area of T-1 from the Rockwell *et al.* (2001) study, we recognized the presence of an abandoned channel to the Kavak River that crosses the fault at a high angle, and is the likely source for the sand exposed in our original T-1 trench. At the fault, sediments in the abandoned channel appear in the aerial photography to splay out southward across the fault, suggesting that a low scarp is present where the fault crosses the channel. We hoped to expose buried elements of the channel system and resolve slip on buried piercing lines, to better constrain the age of these channel deposits, and to further resolve the
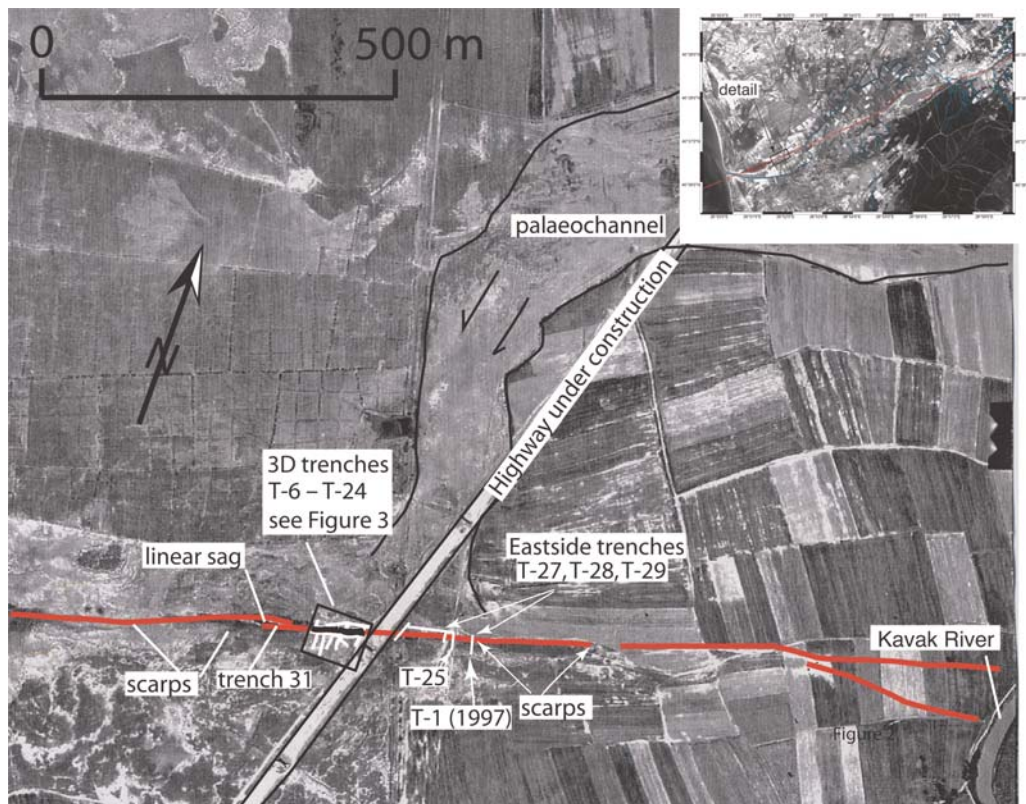

Fig. 2. Annotated aerial photograph of the Saros trench site. Note the Kavak River in the lower right corner of the photo. We trenched in an area that we interpret as a palaeochannel to the Kavak River where it crosses the scarp associated with the NAF. Most trenches are located west of the highway (now completed), with several trenches to the east. The highway was constructed near the thalweg of the main channel and was not open to trenching. The NAF enters the Gulf of Saros 2.6 km west of the highway.
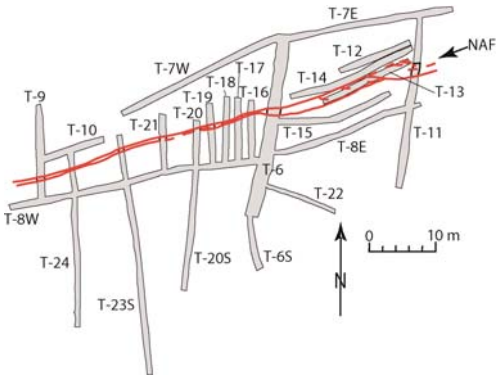
Fig. 3. Map of the 3D trenches on the west side of the highway that were used to resolve lateral slip. The locations of all trenches and fault strands were surveyed with a total station. See Figure 2 for location. The GPS coordinate of the intersection of trenches T-6 and T-8 is 40.6104°N, 26.8643°E.

number of earthquakes that affect the buried sand channel sediments. Towards this aim, we focused our efforts on the margins of the channel and excavated a total of 26 trenches across and parallel to the fault (Figs 2 and 3). The central part of the channel is now occupied by an elevated highway and berm and was no longer available for study.

Several of the trenches that contained important information on past surface ruptures were logged in detail on photographs and later entered into the computer in rectified form. Many of the trenches, however, were excavated for the sole purpose of tracing out the distribution of the distinctive well-sorted sand body (unit 200); data were collected on the thickness of the sand in these trenches but they were not logged in detail. All trench locations, including sand thickness control points, were surveyed with a Wild TC-2000 total station, and all have the same reference elevations established by surveyed horizontal string lines. Further, all critical contacts and relevant stratigraphic pinch-outs were surveyed to precisely locate them in 3D space.

Site stratigraphy

All of the trenches exposed a similar succession of young sediments, with or without the distinctively clean, well-sorted channelized sand. Figure 4 is a detailed log of the east face of trench T-6, and shows the typical stratigraphy of the site, with unit 200 being the distinctive sand that is only exposed on the south side of the fault in this trench. This sand is the same as Unit 3 described in trench T-1 by Rockwell *et al.* (2001), and was also exposed in new trenches near the original T-1 on the east side of the highway (Figs 2 and 5). We use the

lateral distribution of this distinctive sand to constrain cumulative slip on the most recent surface ruptures. In this section, we briefly describe each of the primary units and the associated radiometric control on their ages.

We identified several primary units, along with dozens of secondary contacts, within the section exposed in the trenches. Units are given numeric designations ranging from 10 (topsoil; youngest) to 350 (oldest). Within a given trench, correlation of units both laterally along the trench and from wall to wall is fairly certain, and is based on the character of several distinctive strata contained within the section. Conversely, unit designations in the upper section of T-6 may be generally similar to those in the trenches east of the highway, but their correlation is by inference because we did not connect trenches between these sites (because of the highway). Thus, unit 100 at T-6 may not be exactly the same stratum as unit 100 in the East Saros trenches, although it is similar in character and falls in the same part of the section. The only unit which we feel confident to be the same in all exposures is the distinctive well-sorted sand of unit 200. Even this unit, however, may have some variance in age across the overall study area (few decades or less?) as the sand in the eastern group of trenches was associated with the main palaeomeander channel deposits, whereas the sand at T-6 was deposited by a secondary tributary overflow channel, also associated with the palaeo-meander shown in Figure 2, as discussed later.

The deepest (oldest) logged stratum, unit 350, was exposed at a depth of about 1.5 m on the north side of the fault in T-6, just above the water table. Units 210 to 350 are generally fine-grained silt and clay strata interpreted as a succession of overbank deposits related to the main Kavak River. The only age control for this part of the section is from two dates on a split sample (T6-6) from near the base of this section that yielded consistent calibrated ages of about one to two centuries BC (Table 1). As this sample could have been reworked or have been resident in the system for some period of time, this represents a maximum age for this part of the section.

We use Unit 200 to constrain lateral slip. The sand is channelized and its distribution is locally restricted or absent. In our analysis of the aerial photography (Fig. 2), we interpret an abandoned or tributary channel to the Kavak River as the primary source for this sand. Within this palaeo-channel system, we exposed the sand in most of the trenches and can make some general observations about its extent.

East of the highway, the sand fills a major, broad channel, and the sand is locally over 1 m thick. We excavated a trench parallel to the fault between T-25 and the highway, and the sand locally extended to
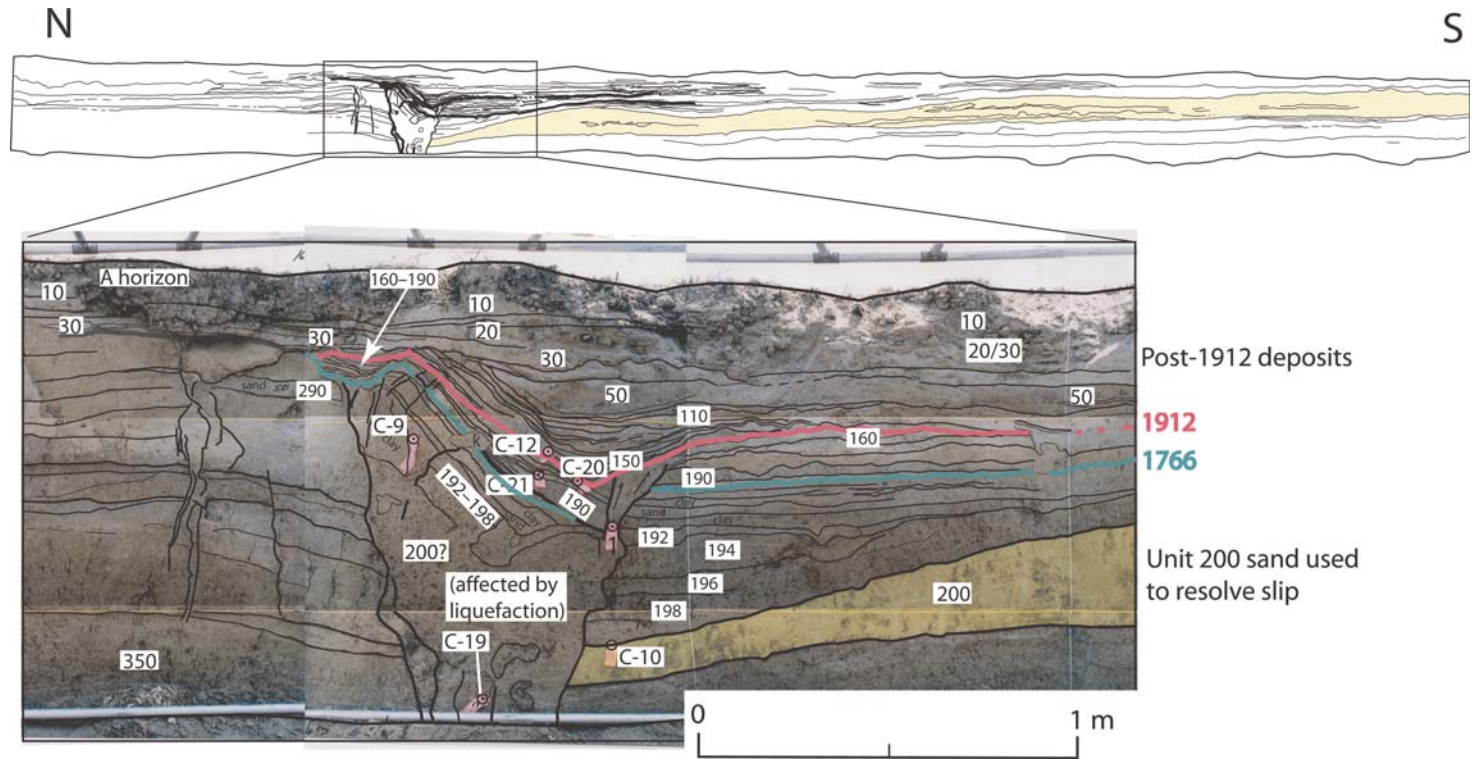
Fig. 4. Log of the east face of trench T-6. Units are described in the text. The labels 1912 and 1766 correspond to the thicker black contacts and represent the 1912 and 1766 event horizons, respectively. The unit 200 sand is the stippled grey unit in the top diagram.
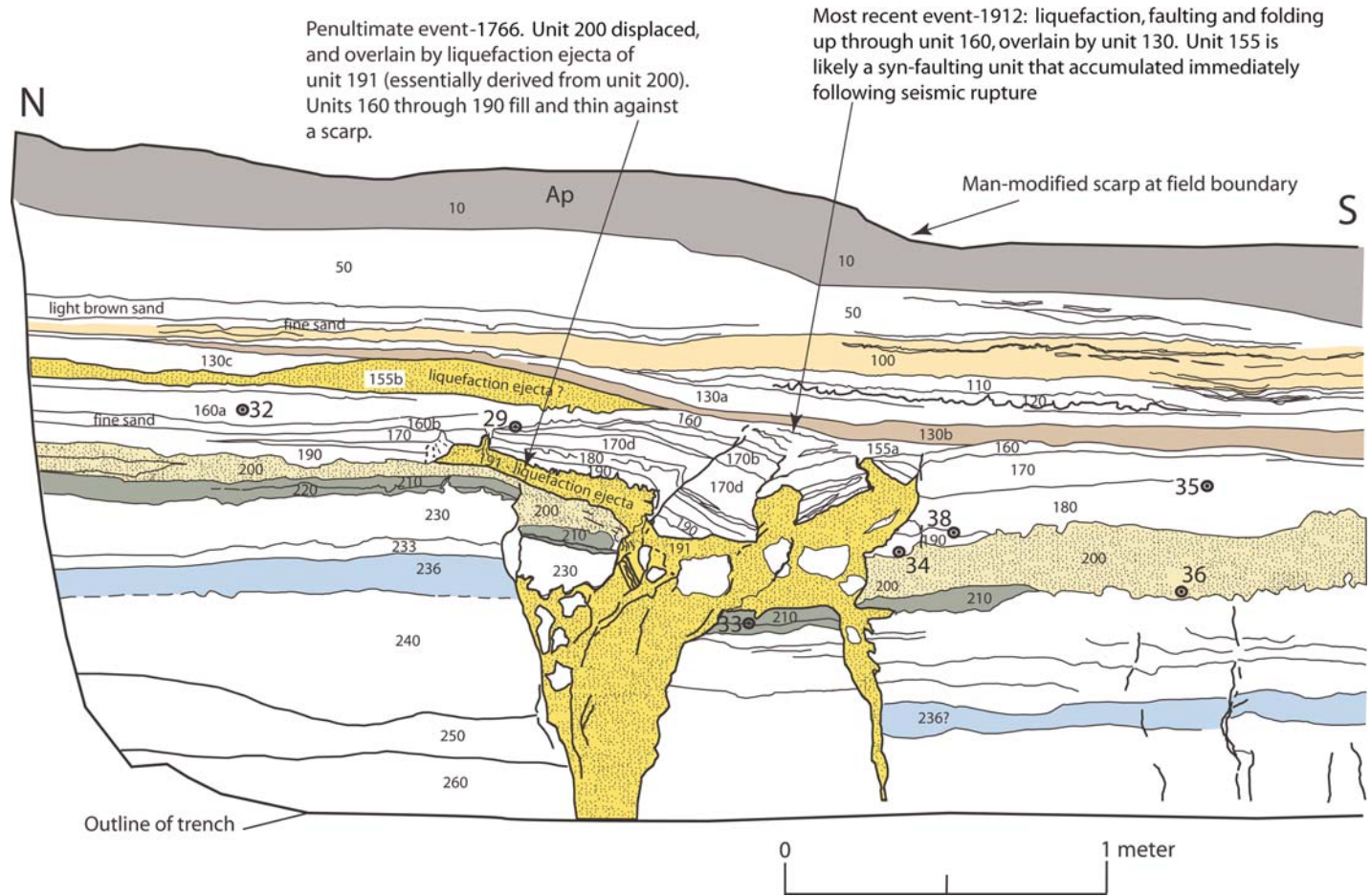
Fig. 5. Log of the east face of trench T-25, west side of the highway. Units are described in the text. Charcoal collection points are indicated as black dots.

Table 1. *Radiocarbon dates from trenches at Saros, the Ottoman Canal, and Köseköy*

CAMS #	Sample name	Trench exposure	Notes	Unit	$\delta^{13}C$	Fraction modern	$\pm$	$D^{14}C$	$\pm$	^{14}C age	$\pm$	Calibrated age range (2σ)
Kavakköy and Saros			**Trenches**									
67291	K-T14-48	Proxy to T6		92	−25	0.9556	0.0048	−44.4	4.8	360	50	AD 1451–1642
67290	K-T6-46	T6	0.15 mgC	95	−25	0.8972	0.0053	−102.8	5.3	870	50	AD 1041–1267
67285	K-T6-12	T6E		c. 99	−25	0.8401	0.0042	−159.9	4.2	1400	40	AD 592–703
67289	K-T14-45	Proxy to T6		102	−25	0.9675	0.0043	−32.5	4.3	270	40	AD 1489–1955
67288	K-T14-44	Proxy to T6		105	−24.3	0.9038	0.0043	−96.2	4.3	810	40	AD 1170–1285
67696	K-T13-32	East Saros, East wall		150	−25	0.9698	0.0048	−30.2	4.8	250	50	AD 1489–1955
67694	K-T13-29*	East Saros, East wall	0.12 mgC	base 160	−25	0.9232	0.0065	−76.8	6.5	640	60	AD 1282–1414
67698	K-T13-35	East Saros, East wall		top 180	−25	0.8855	0.0033	−114.5	3.3	980	40	AD 999–1164
68212	K-T13-41	East Saros, East wall	shell	180	0	0.8711	0.0043	−128.9	4.3	1110	40	AD 874–1016
67697	K-T13-34	East Saros, East wall		190	−25	0.9467	0.0048	−53.3	4.8	440	50	AD 1408–1631
67286	K-T6-43	T6W @ M9		200	−25	0.9777	0.0053	−22.3	5.3	180	50	AD 1655–1955
67284	K-T6-3	T6E		200	−25	0.9682	0.0042	−31.8	4.2	260	40	AD 1513–1955
67292	K-T6-43	T6W @ M9	0.04 mgC	200	−25	0.9931	0.016	−6.9	16	60	130	AD 1529–1955
67695	K-T13-30	East Saros,West wall		210	−25	0.9662	0.0048	−33.8	4.8	280	40	AD 1488–1955
67293	K-T6-6	T6E		310	−27.6	0.7638	0.0034	−236.2	3.4	2160	40	360–60 BC
67287	K-T6-6	T6E		310	−25	0.771	0.0034	−229	3.4	2090	40	190–2 BC
Ottoman Canal Berm		(dated at the Arizona AMS facity)										
AA33511	Berm 14C-3	Tepetarla Berm Trench			−25.6	0.9193	0.0055			675	50	AD 1274–1402
AA33512	Berm 14C-7	Tepetarla Berm Trench			−25.2	0.7815	0.0053			1980	55	112 BC–AD 191
AA33513	Berm 14C-8	Tepetarla Berm Trench			−24.7	0.7976	0.005			1815	50	AD 85–371
AA33640	Berm 14C-5	Tepetarla Berm Trench			−25.7	0.7985	0.0047			1805	45	AD 120–373
Köseköy Trench 1												
68683	T1-19	Above E2		3b	−25	0.9809	0.0043	−19.1	4.3	150	40	AD 1670–1955
68684	T1-6	Below E2		4	−25	0.9526	0.0043	−47.4	4.3	390	40	AD 1441–1634
68686	T1-27			5c	−25	0.976	0.0047	−24	4.7	200	40	AD 1647–1955
68685	T1-25			7	−25	0.9922	0.0048	−7.8	4.8	60	40	AD 1688–1927
68687	T1-23			10	−25	0.8183	0.004	−181.7	4	1610	40	AD 381–555
68688	T1-16			11	−25	0.8281	0.004	−171.9	4	1520	40	AD 444–630

below the depth of the 2-m-deep trench. This was an exploratory trench to determine the character of the sand and was not logged in detail because of safety constraints. Nevertheless, it was clear to us that the primary fluvial channel lies east of or beneath the highway, and our trench T-25 was located near the margin of this system. Trench T-1 of Rockwell *et al.* (2001), which lies within 10 m to the east of T-25, also exposed this sand unit (unit 3 in their trench log).

West of the highway, unit 200 is substantially more restricted in its areal extent. North of the fault, the well-sorted sand is restricted to a narrow and shallow (<20 cm) 'feeder' channel that flowed southward across the fault. South of the fault, the sand thickens dramatically and locally reaches over 40 cm in thickness. We collected observations on the sand thickness in all exposures to provide a basis for developing an isopach map of the sand (Fig. 6). We collected these observations at a maximum spacing of 50 cm and tied all

measurements to a common, surveyed system of horizontal string lines. We also measured the absolute elevations of the top and bottom of the sand relative to the string datum to provide a complete spatial reference. These data are presented later to resolve slip on the channel fill of unit 200.

The age of unit 200 is constrained to be younger than AD 1655. We dated several samples from this unit (Table 1), along with those above and below it, and use the youngest date to constrain its maximum age. Several other dates from unit 200 also fall in the same time period, but because of larger uncertainties, can only be constrained to the period from about 1490–1530 to the present (1955). All of the samples constrain the sand to the past 500 years, but sample T6-43, recovered from stratified alluvium within the channel, can be no older than AD 1655 and may be considerably younger. This, of course, assumes that this sample is in stratigraphic context, but as the deposit is well-stratified and there was no evidence otherwise,
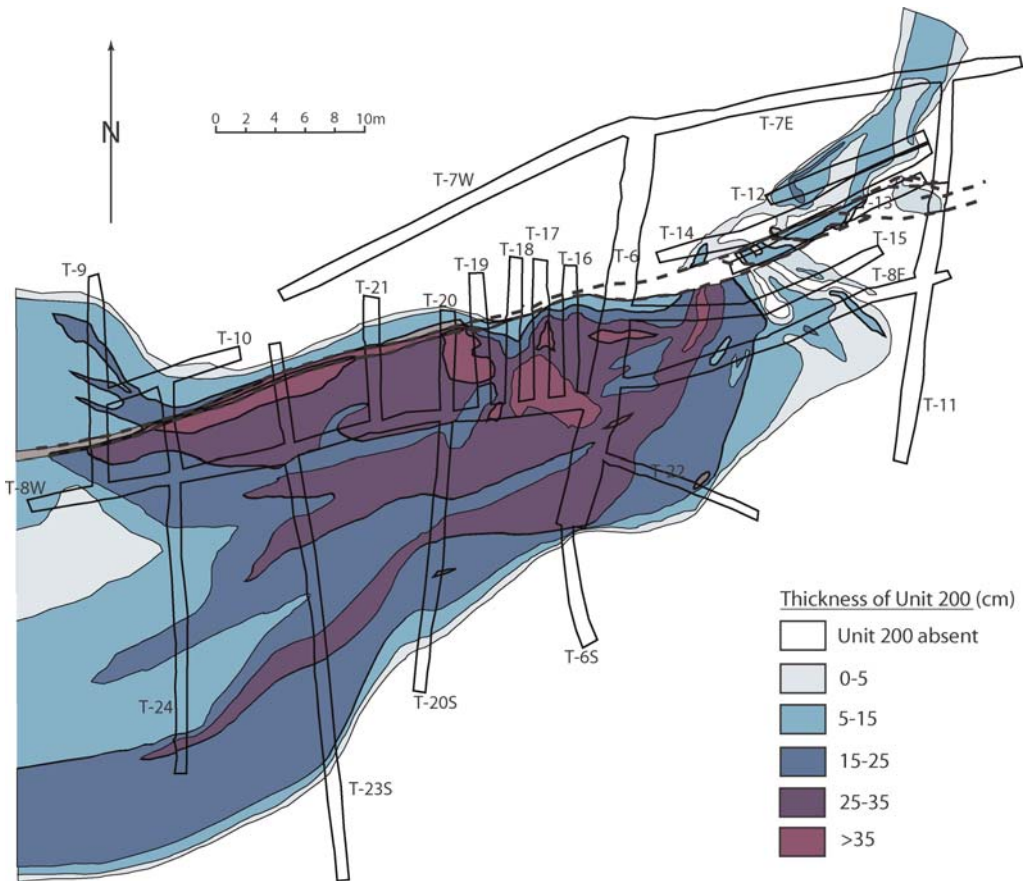

Fig. 6. Isopach map of the unit 200 sand, based on nearly 1500 measurements. Note the current location of the feeder channel relative to the fan apex.

we take this to be the case. Thus, we interpret all of the radiocarbon samples that lie above this unit and that have older apparent ages to be the result of either reworking of detrital charcoal or, more likely, the consequence of the charcoal (and its original wood) having been resident in the system for some period of time. The post-1655 date places strong constraints on which earthquakes may have produced surface rupture at this site and contributed to the observed amount of offset on unit 200, as discussed below.

The stratigraphic units above unit 200 can be designated as either sedimentation within the fault zone, possibly due to formation of a depression along the fault, or the result of overbank sedimentation by the Kavak River and its tributary channels. Units 192 to 198, recognized in the east face of T-6 (Fig. 4) and in adjacent trenches to the west, are interpreted to be a sequence of fine-grained deposits that fill a narrow trough between the unit 200 fan and a low fault scarp. Although this may be interpreted as the result of deformation along the fault, there is no direct evidence for a surface rupture in this part of the section. There is a reasonable interpretation, however, that invokes purely stratigraphic mechanisms to produce this deposit: the isopach map of the sand in Figure 6 clearly shows a fan that splays out and flows west, parallel to the fault, thereby producing a slight low along the fault. Thus, there is no need to require a faulting event to produce this low, and we prefer the non-faulting interpretation.

In contrast, units such as 110 to 150 in trench T-6 fill a depression that formed immediately after a surface rupture, as indicated by faulting and fissuring up to the base of that section. In these cases, the units may be only very locally preserved along the fault, although their significance to the interpretation of the event stratigraphy may be profound.

Units 10 to 100 are sandy to silty sediments that bury the fault scarp and are presumably derived from flood events from the Kavak River. Unit 10 is the A horizon developed in this uppermost section and is also the active plough pan in areas that are farmed, such as to the east of the highway. We dated a number of detrital charcoal samples from units 10 to 190 to provide preliminary constraints on the age of the overall section. Because unit 200 was found to be younger than AD 1655, all higher units must be as well. The radiocarbon results demonstrate a variety of dates ranging between about AD 600 and 1955 (i.e. the present), with no particular order in the section. We interpret all of these as having had a small to large component of resident age prior to their incorporation into the sediments exposed in our trenches. From this, we interpret the entire section from unit 200 to the surface as being deposited during the

past 350 years or so. As this corresponds to the part of the C-14 calibration curve that cannot be resolved without very precise ages, we did not pursue further dating of this section.

Evidence for earthquakes

There was evidence observed for two large surface ruptures in nearly every trench that we excavated across the fault. In many of these, there were two deposits of well-sorted fine sand that appear to have been ejected out of the fault zone and derived from unit 200. In trench T-25 (Fig. 5), we designate the earlier of these ejecta deposits as unit 191. We also observed structural evidence for two surface ruptures, with faults and fractures extending up to a specific stratigraphic level and then being overlain by unfaulted deposits. We did not construct detailed trench logs of most exposures due to the lack of time and because our focus for many of these trenches was to map out the extent of unit 200. Nevertheless, both T-6 and T-25 record both of these events and are discussed herein.

Evidence from trench T-6. The fault in T-6 is narrow, less than 0.5 m at the base of the trench. Within this fault zone, faulting has produced liquefaction, brittle faulting, tilting, fissures, and a narrow trough into which sediment accumulated. The interpreted event horizons for each of these phenomena are coincident and correspond to the base of unit 190 and the base of unit 150.

In T-6E (east wall of trench T-6), fractures extend to the base of unit 190 and are overlain by well-bedded stratigraphy of units 160–190. Within the fault zone, a massive, well-sorted fine sand that is clearly affected by liquefaction is likely derived from unit 200, or possibly another sand below the base of the trench. This liquefaction sand is also overlain by unit 190 along both margins of the fault zone in this exposure. Finally, along the northern edge of the fault zone, a narrow depression is filled by finely laminated stratigraphy of units 160–190. We interpret the depression to be formed as a direct result of surface rupture.

The most recent event, 1912, is represented by rupture and liquefaction of units 190 up through 160 to the base of unit 150, and tilting of these units within the fault zone. Units 110 to 150 accumulated within a trough along the fault and are draped across the scarp. Unit 50 largely fills against the scarp, and units 10–30 were deposited after the scarp had been completely buried.

Evidence from trench T-25. East of the highway, we constructed detailed logs of the fault zone in trench T-25 to further constrain the timing and number of events that post-date the unit 200 sand. It should

be noted that the earlier study by Rockwell *et al.* (2001) also found evidence for only two surface ruptures after deposition of their Unit 3, which is identical to unit 200 described herein. Trench T-25 lies within 10 m of Rockwell *et al.*'s (2001) trench T-1.

In the east wall of T-25, the northernmost fractures extend up through unit 200 and are overlain by another clean sand (unit 191) that we interpret as ejecta derived from unit 200. Massive clean sand fills the main fault and is also interpreted to be the result of liquefaction of unit 200. Overlying unit 191 is a sequence of bedded silt and sand units (units 160 to 190) that are not faulted by the northernmost strand of the zone. These observations all indicate a surface rupture that occurred when unit 200 was at the surface in this area.

Another set of fractures displaces all units up through 160, including unit 191 (liquefaction sand from the penultimate event). Chunks of bedded stratigraphy, composed of units 160 to 190, lie floating within the fault zone in a massive, fine sand matrix that we interpret as the result of re-liquefaction of the unit 200 sand. Unit 155a fills the trough in the fault zone and appears to be derived from unit 160, whereas unit 155b is a well-sorted sand that is identical to the unit 200 sand, has the form of a sand-blow, and is likely a second ejecta unit associated with the 1912 earthquake. All of these deposits are overlain by undeformed strata of units 100 to 130, which fill against the scarp, and units 10 to 50, which bury the scarp. The apparent scarp at the surface is evidently man-made.

The above observations indicate that there are two surface ruptures preserved in the stratigraphy, one at the contact at the base of unit 190 and one between deposition of units 130 and 155. These are identical to the relationships determined in trench T6 and we interpret these to be the same two events. Thus, at these and all other exposures that we examined in our field exercise, we noted evidence for two ruptures that produced liquefaction, surface faulting, and consequent sedimentation along the fault. Both of these events must have occurred after deposition of the channel sand of unit 200, or after AD 1655. The only two large events that may be ascribed to these surface ruptures are the large regional events of August 1766 and August 1912 (Ambraseys & Finkel 1987*a*, *b*, 1995; Ambraseys 2002*a*; Rockwell *et al.* 2001). Thus, we attribute lateral slip on unit 200 to be the cumulative result of these two earthquakes.

Determination of lateral slip

The channelized nature of unit 200 is ideal for resolving cumulative slip for the two events that post-date its deposition. From the aerial photographic analysis, it appeared that the palaeochannel containing unit 200 flowed at a high angle to the fault. We chose the area west of the highway to conduct the detailed 3D portion of this study because the area is devoid of agriculture and we were unrestricted in our ability to excavate long trenches both across and parallel to the fault zone.

In the preliminary excavations, such as trench T-6, we were not certain of the areal distribution of the unit 200 sand, so we began fault-parallel excavations to determine its extent. In all, we excavated 19 trenches and trench extensions to resolve the geometry of the unit 200 deposit. All exposures were surveyed with a Wild TC 2000 total station to provide accuracy. Further, a surveyed string line was emplaced in all trenches at the same elevation to assure accurate measurement of the sand thickness and the relative elevations of its top and base. We took over 1500 detailed measurements on the thickness of the sand, including the exact locations of the pinch-outs, to construct an isopach map of its distribution (Fig. 6).

Unit 200 is much thicker on the south side of the fault than on the north. We take this to indicate that a low scarp was present at the time the channel flowed across the fault. North of the fault, the sand is confined to a narrow channel and never exceeds 20 cm in thickness. The channel slopes to the south, towards the fault, and then thickens to over 40 cm where it crosses the fault. The overall form is that of an alluvial overflow fan, and we interpret the channel to have splayed at and beyond the fault scarp, resulting in deposition of the main fan on the south side. The fan is deflected downstream, towards the coast to the west, and its true SE side only extends south of the fault for 5–10 m. As seen in trench T-6, the fan has a convex-up profile in cross-section and is multi-lobed. The apex of the fan is exposed in trench T-15, and the fan rapidly thins to the east and pinches out in trenches T-8 and T-15. To the west, the fan is bounded on the north by the fault for a distance of about 30–35 m, and then the edge of the fan crosses the fault with 10–15 cm of deposition north of the fault. In the vicinity of T-6 and the area of the feeder channel, unit 200 is thickest away from the fault except at the fan apex.

We reconstruct the fan apex with the deepest portion of the feeder channel to resolve about 9 m of lateral slip (Fig. 7). A secondary smaller channel *c*. 8 m west of the main channel also reconstructs to a secondary fan apex, and the margins of the fan to the east of the feeder channel all realign. Furthermore, the thickest portion of the fan that ponded adjacent to the fault west of T-6 realigns to the thinner section of sand that spilled across the fault to the north, although this latter match is not tightly constrained. The uncertainty in the 9 m estimate is on the order of about 1 m, based on the
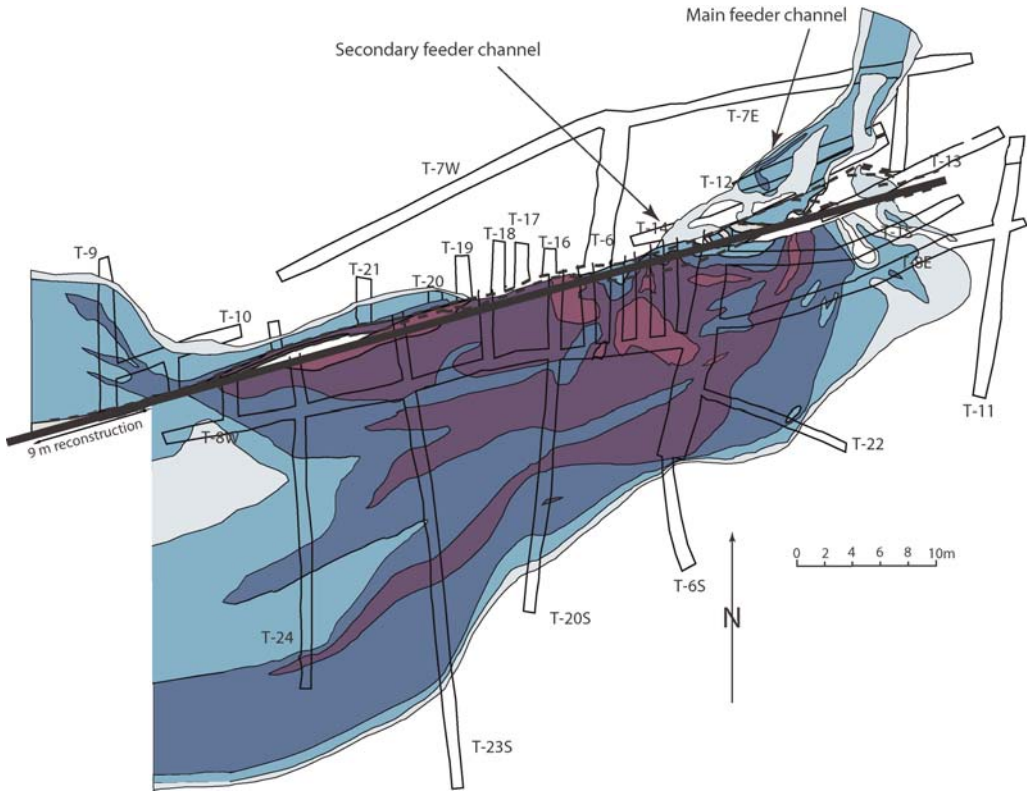
Fig. 7. Reconstruction of the fan apex with the thalweg of the feeder channel. Slip estimated at about 9 m, with about 1 m of uncertainty. Note that the eastern margin of the fan complex, along with a secondary feeder channel in T-14, also all realign with 9 m of reconstruction.

realignments and their mismatches if the reconstruction is less than 8 m or greater than 10 m. We take this 9 ± 1 m value as the cumulative slip produced by both the 1766 and 1912 earthquakes. If each earthquake produced similar slip at this site, then the c. 4–5 m of presumed slip agrees well with the estimated 1912 slip measured by Altunel et al. (2004) and Altınok et al. (2003) along the central and eastern onshore portions of the Ganos fault based on deflected roads and field boundaries, with their measurements located 15 to 50 km east of our study site. It is also similar to the average values for many of the large earthquakes that have ruptured the North Anatolia fault this century, and is consistent with the amount of slip predicted by Ambraseys & Finkel (1987a) for the 1912 earthquake, based on its inferred magnitude of about M7.4.

Timing of the past four events

The 1912 and 1766 earthquakes almost certainly produced the last two recognized surface ruptures in the Saros area. In our earlier study, we recognized evidence for two additional ruptures, but we did not have sufficient radiometric data to constrain their timing (Rockwell et al. 2001). In this paper, we combine all of the radiocarbon data and event evidence from both studies to better constrain the timing of the rupture history for the past 1000 years or so. For this task, we first compiled the radiocarbon dates from each trench that constrain the timing of the past four recognized events. There are clearly some dates that have substantial residency or inheritance, likely due to the burning of old wood. We therefore take only the dates from each section that did not result in stratigraphically inverted radiocarbon dates (Table 2).

We placed the radiocarbon dates in Table 2 in stratigraphic sequence in OxCal (Ramsey 2000) and analysed them for the inferred ages of the four events. Using 1912 as the most recent event and entering this as a calendar date in OxCal, the other three events are plotted as probability density functions (pdfs) of the likely age range at 2σ (Fig. 8). Event E2 plots in the appropriate timeframe for the 1766 earthquake, which we take as a

Table 2. *Radiocarbon dates used to constrain the timing of the past four Ganos fault ruptures at the Kavak–Saros site*

Sample name	Trench/unit	^{14}C date	Calibrated age range	Reference
K-T14-4S	T14/102	270 ± 40	AD 1489–1955	This study
Event E1 (1912)				
K-T13-32	T25/150	250 ± 50	AD 1489–1955	This study
Event 2 (1766?)				
K-T6-43 split	T6/200	60 ± 130	AD 1529–1955	This study
K-T6-43	T6/200	180 ± 50	AD 1655–1955	This study
K-T6-3	T6/200	260 ± 40	AD 1513–1955	This study
14C-4	T1/2b (base 200)	440 ± 60	AD 1446 (1405–1529 @ 0.73) (1542–1634 @ 0.27)	Rockwell *et al.* (2001)
14C-5	T1/3b (*c.* 240)	530 ± 45	AD 1415 (1308–1358 @ 0.20) (1381–1451 @ 0.80)	Rockwell *et al.* (2001)
Event 3				
T5 14C-1	T5/G5	1010 ± 45	AD 1020 (965–1163)	Rockwell *et al.* (2001)
Event 4				
T5 14C-31	G5/H1	1290 ± 60	AD 755 (657–881)	Rockwell *et al.* (2001)
T5 14C-7	H1	1285 ± 45	AD 743 (664–825 @ 0.93) (833–865 @ 0.07)	Rockwell *et al.* (2001)
T5 14C-26	base H	1135 ± 45	AD 894 (791–1003)	Rockwell *et al.* (2001)

confirmation of that inference. Event E3 is more broadly constrained to the period from about AD 1000 to 1450, but fits the timeframe of the 1344 or 1354 earthquake very well. Event E4 is slightly better constrained in its timing, with a peak distribution around AD 900–1000 and a maximum calibrated range of about AD 750–1150. However, considering that the majority of radiocarbon dates displayed some residence age, either due to time in the system or burning of old wood, it is likely that the dates that constrain these older events also have some inheritance. If so, then the actual dates of the events may be younger, or at least fall in the younger portion of the distribution.

Ambraseys & Finkel (1987*b*) document large events in this region in 1063 and 1542, and a sequence in 1343–1354 (with 1344 and 1354 being to the west). The 1542 event was placed by Ambraseys & Finkel (1995) in the spurious category, and Ambraseys (2002*a, b*) totally ignores this event in later work, so we discount this as a likely candidate for one of the four events.

Based on the available radiocarbon data, we interpret E3 as likely being the 1344 or 1354 earthquake. The 1343–1354 sequence appears to have been a progressive rupture from the Marmara Sea to the Gulf of Saros (Ambraseys & Finkel 1991), with the 1354 being the farthest west and possibly the most destructive (and presumably the largest). Based on their tentative locations, however, E3 could correspond to either the 1344 or 1354 events.

Event E4 is most likely the AD 1063 earthquake, as there are no other obvious candidates.

The average recurrence interval for ground ruptures at Saros is about 250–300 years if one takes four events in the past 1000–1200 years. A better way to frame recurrence is to take the intervals between earthquakes and take the mean, thereby also establishing the standard deviation. Using this approach, and taking the event ages as discussed, yields three intervals (146 years, 422 years (or 412 years), 281 years) with an average recurrence interval of *c.* 280 ± 110 years. Combined with the average slip per event of 4.5 m for the past two events, and assuming each of the four events displayed similarly large displacement, we estimate the slip rate at $15.9(+10/-4.5)$ mm/a. We emphasize, however, that this rate is strongly dependent on our assumption that the earlier two events produced similar displacements as the latter two, and this needs to be tested with future studies. Nevertheless, based on the historically recorded extent of damage, it is unlikely that the earlier events were larger than 1766 or 1912, so this rate is not likely to increase significantly.

Prior to the 1063 earthquake, there are potentially three large events reported for this area back to the fifth century AD. An event in AD 824 event is reported to have 'devastated the Tekirdag coast . . . causing considerable concern throughout Thrace' (Ambraseys & Finkel 1987*b*), and although this may be a candidate, it may have occurred too far
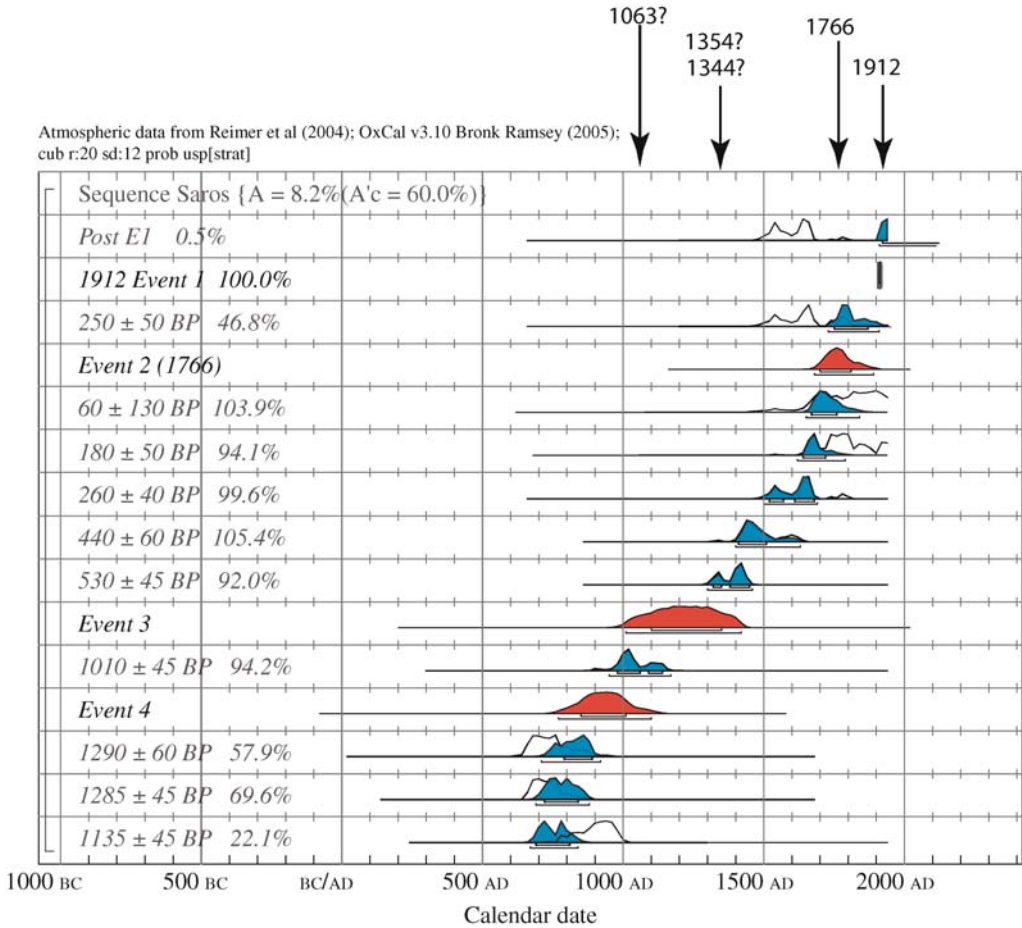
Fig. 8. OxCal plot of the probability density functions for selected (non-inverted) radiocarbon dates from the Saros (this study) and Kavak (Rockwell *et al.* 2001) studies. Note that the pdf for E2 is consistent with the 1766 earthquake. Also note that the earlier pdfs, although not well-constrained, are consistent with earthquakes in 1344 or 1354 and 1063.

to the east. Similarly, an earthquake in AD 542 is located by Ambraseys & Finkel (1991, plotted on their fig. 3) very close to their location for the 1354 earthquake near the head of the Gulf of Saros, but the damage appears to be more to the east in Constantinople (Istanbul). Ambraseys (2002*b*) later discounts this event, and suggests that this may be based on spurious reports. Finally, an event in AD 484 is reported to have been very destructive, with Gelibolu (Gallipoli) completely destroyed (Ambraseys & Finkel 1991).

If we include the 484 and the 824 earthquakes, the average recurrence interval becomes 284 ± 90 years, which is indistinguishable from the shorter-term recurrence interval. Using the average displacement of 1766 and 1912 yields a similar estimated rate of $15.8(+7.3/-3.8)$ mm/a for the past 1600 years if the average slip assumption of *c.* 4.5 m is

used. These estimates assume that: (1) the past $1-1.6$ ka is a long enough period to assess a long-term rate; (2) the historical record of large earthquakes is complete for this area which may not be the case before about AD 1000; (3) the rupture history is complete in our trenches, at least for the past 1000 years; and (4) each event has similar magnitude of displacement as we determined for the average in the past two events. This last assumption is important because we are basing our rate estimate on average displacement and average return period, not a dated feature that is offset a specific number of metres. Consequently, if some events have been very large, then we may underestimate the inferred rate using this method. However, we have likely overestimated the rate if some of these historical events were smaller than 1766 or 1912, which may have been the case for the 1344, 824 and 484

events. It is noteworthy that this rate is below the *c*. 24 mm/a (and possibly as high as 26−28 mm/a) measured by GPS for the NAF (McClusky *et al.* 2000; Reilinger *et al.* 2006), although the higher rate is allowed at the uppermost range of our estimate from the palaeoseismic data.

Palaeoseismology of the Izmit to Sapanca segment

We initiated palaeoseismic studies along the Izmit–Sapanca fault segment in October 1998 prior to the 1999 earthquakes. In our preliminary work, we focused on dating a faulted canal feature that we knew at the time to likely be the result of an effort by the Ottomans in 1591. After the earthquake, we returned to the canal to resolve how many earthquakes had affected the canal stratigraphy. We also began trenching west of the end of the canal along a small fluvial channel in the township of Köseköy with the purpose of resolving a longer record (Fig. 9). As will be shown, the records at

both sites are similar and only record fault activity for the past 400 years or so.

The Ottoman canal site

Multiple periods of canal construction have been discussed in the literature (Finkel & Barka 1997), with at least two known excavation efforts. The earliest effort is pre-Roman and was intended to connect Lake Sapanca with Izmit Bay, thereby opening up commerce and access to the inland forests and other resources. A number of subsequent efforts were 'discussed' (mentioned in court records, etc.) although most of these were never undertaken. The most recent effort, for which there is direct historical documentation and known expenditures, was undertaken by the Ottomans in 1591 (Finkel & Barka 1997). In a preliminary effort in 1998, we excavated the southern margin of a large, abandoned canal at Tepetarla with the purpose of dating the construction of this prominent feature, which crosses the fault zone between Tepetarla and Köseköy. The canal extends from near Lake
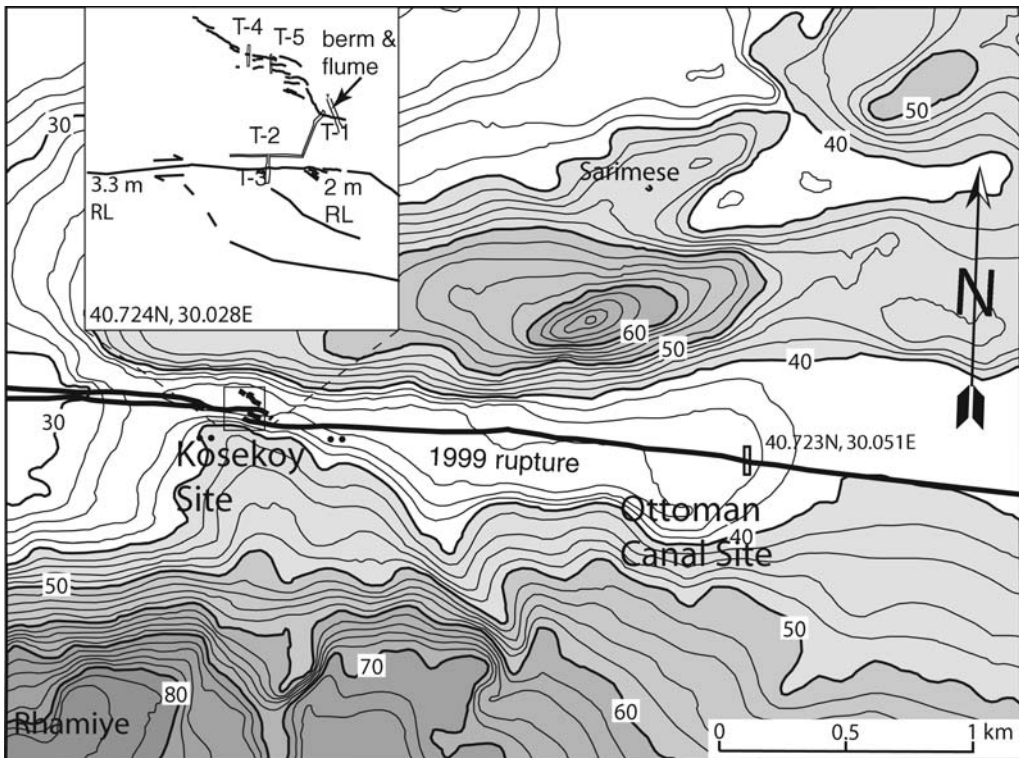

Fig. 9. Map of the Köseköy and Ottoman canal sites near Sarimeşe. The inset shows a detail of the Köseköy trenches whereas only a single trench was excavated at the canal site. The 1999 coseismic lateral displacements (Barka *et al.* 2002; Rockwell *et al.* 2002) along the fault at Köseköy are indicated in the inset.

Sapanca westward about half of the distance to Izmit Bay, consistent with historical accounts for the 1591 effort. The purpose of our initial trench was to resolve whether this was the Ottoman effort of 1591 or an earlier canal effort.

We found numerous pieces of small to large detrital charcoal, some that were associated with burn zones, that we interpret to represent cooking fires or fires to boil water for tea (as is a common practice today in Turkey). We collected eight large samples and dated four of the samples to place maximum ages on the berm construction, and therefore the canal excavation project. In that it is likely that the workers burned dead wood for their fires, and as there are numerous large trees in the area today, we surmise that all of the samples are likely older than the actual age of the berm. As it turns out, the ages of the detrital charcoal pieces range from a maximum age of 112 BC to as young as AD 1402 (Table 1). We therefore infer the berm and canal construction to post-date the youngest fourteenth century date, and to be the effort funded by the Ottomans in 1591. Thus, all of the alluvial fill within the canal must date to younger than 1591

so we did not attempt further C-14 dating in the canal fill.

In the summer of 2000, we excavated a trench across the 1999 rupture west of Lake Sapanca where the fault is entirely contained within the canal fill (Figs 1 and 9). The trench site was chosen about 2 m west of a small several-metre-long open extensional fissure resulting from a *c*. 2 m-wide releasing step-over. The trench exposed predominantly fine-grained, bedded clay-rich canal fill, although a distinctive sand was found to fill a fissure zone within the fault zone, apparently resulting from a prior rupture (Fig. 10). The fault zone is approximately 3 m wide in the trench, although the 1999 rupture zone is narrower.

The stratigraphy was differentiated into nine units, with the topmost and youngest unit (unit 1) interpreted as a plough pan. Unit 1 is a massive, organic-rich silty clay, similar in texture to several of the underlying strata. Unit 2, which is bedded and further subdivided into several subunits, is in part an alluvial fill within the fault zone. Unit 2a is a fine silty sand that is only present north of the 1999 rupture trace. Unit 2b is clayey silt that fills a
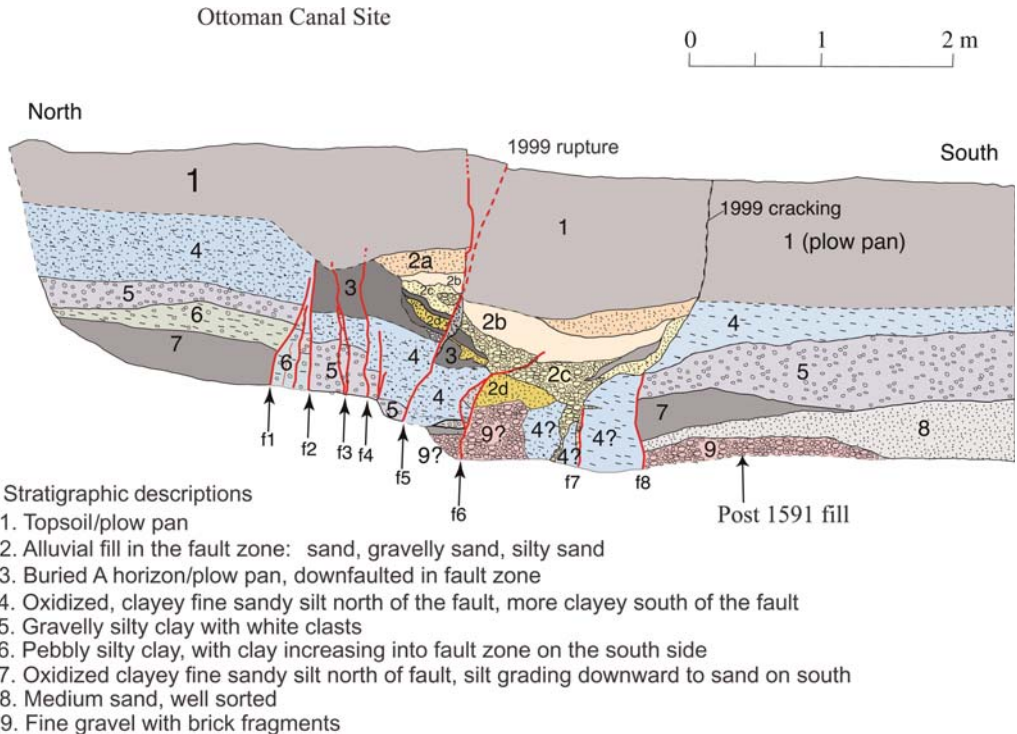

Stratigraphic descriptions
1. Topsoil/plow pan
2. Alluvial fill in the fault zone: sand, gravelly sand, silty sand
3. Buried A horizon/plow pan, downfaulted in fault zone
4. Oxidized, clayey fine sandy silt north of the fault, more clayey south of the fault
5. Gravelly silty clay with white clasts
6. Pebbly silty clay, with clay increasing into fault zone on the south side
7. Oxidized clayey fine sandy silt north of fault, silt grading downward to sand on south
8. Medium sand, well sorted
9. Fine gravel with brick fragments

Fig. 10. Trench log of the Ottoman canal site near Tepetarla. The 1999 rupture produced slip in a narrow zone, with minor cracking over a 2 m width. All deposits exposed in the trench post-date the excavation age of the canal in AD 1591.

depression within the fault zone. In contrast, unit 2c is a coarse gravelly sand that not only fills the depression in the fault, but also extends downward in the fractures to the base of the trench. This unit grades upward into sand at its top. Unit 2d is well-sorted fine-grained sand, and we interpret this unit to be the result of liquefaction; it is likely derived from a clean sand below the base of the trench. Units 2a to 2d may constitute a fill sequence in a fissure within the fault zone following an earthquake.

Unit 3 appears to be an organic-rich, buried topsoil unit that was incorporated into the fault zone and is bounded by fault strands from an earlier event. Unit 4 is a massive, pebbly clay to clayey sandy silt (varies laterally) that grades down to the pebbly silty clay strata of units 5 and 6. These units are interpreted as quiet-water canal-fill alluvium, although the presence of scattered pebble clasts may alternatively suggest a debris flow origin. Unit 7 is an oxidized, finely bedded silt that grades downward to sand, whereas unit 8 is a well-sorted sand. Unit 9 is a sandy gravel of probable fluvial origin, and units 9 to 7 apparently represent a fining-upward fluvial sequence. The unit designated as '9?' within the fault zone is lithologically similar to both unit 9 and unit 2c and may be part of the section that liquefied or was mobilized during liquefaction of unit 9.

We did not directly date any of the strata within this trench using radiocarbon, although detrital charcoal was abundant and we collected over 50 samples from this trench. However, as the base of the canal was not encountered (the base should be greater than 5 m depth as the site is about 4–5 m above the elevation of Lake Sapanca), we infer the entire section to post-date AD 1591. In that many or most samples likely have some residence age (growth plus burning prior to burial), and because of problems with calibrating C-14 dates after about AD 1600, we did not see the utility in spending the effort to further date the section. Nevertheless, all earthquakes recorded at this site must also post-date AD 1591, which is fairly well-recorded in the history for this region.

Evidence for prior earthquakes

There is clear structural and stratigraphic evidence for at least one and probably two events prior to that of 1999. For discussion purposes, we have numbered the individual fault cracks as f1 to f8, from north to south. In a couple of cases, minor faults are grouped with more major ones. Several of these faults moved in at least one prior event, whereas only two appear to have been reactivated in 1999, which is referred to as event E1.

The 1999 (E1) rupture localized along a narrow crack, fault f5, near the centre of the trench. E1 displaces all strata up through unit 1 to the surface. A second surface crack aligns with fault f8, and this fault becomes the edge of a 2-m-wide pullapart that produced a narrow sag in 1999 only 2 m east of this trench face. In the trench wall, this fault appears to have only cracked, and no evidence of any significant displacement could be resolved. The base of the soil may be offset by a couple of centimetres, but that was not clear. Below the cracked soil, however, fault f8 defines the southern edge of the fault zone and was clearly active and a major fault in an earlier event. Along fault f5, the principal 1999 displacement surface, different units are juxtaposed and similar units have significant variations in thickness across the fault. We attribute these relationships to the *c.* 3 m of lateral slip recorded for the 1999 earthquake in this vicinity (Rockwell *et al.* 2002).

At least one earlier event, E3, is strongly indicated by the occurrence of a number of fault strands that break units 3–9 but are overlain by the unbroken soil of unit 1. Fault f2 drops an older topsoil horizon, unit 3, down against units 4 and 5, and the mismatch in unit thicknesses across this fault suggests substantial lateral slip. Faults f1, f3 and f4 also cut units 3 to 7 but are overlain by unit 1. There is no indication that any of these faults were activated in 1999. Faults f6, f7 and f8 also appear to have activated in this earlier event, which apparently resulted in an open fissure at the surface that was subsequently filled by unit 2. Unit 2d is a fine-grained sand that may be the result of a sand blow. Unit 2c, in contrast, is a gravelly sand that is intrusive downward into the fault zone and is very similar to the sandy gravel of unit 9. We observed gravelly sand mobilized during the 1999 earthquake, resulting from liquefaction and lateral spreading on the lake shoreline at Sapanca, so we surmise that this gravel may also be a consequence of liquefaction, in spite of its coarse grain size. In any case, the occurrence of the unit 2 deposits precisely within the fault zone virtually requires that an open fissure was present after deposition of unit 4 and the development of the soil of unit 3. We attribute the presence of the unit 2 deposits to this earlier faulting event.

A third event that is intermediate in age between events E1 and E3 is suggested by the breakage of the unit 2 fill by fault f6, which juxtaposes units 2d and 4, and causes a significant mismatch in the thickness of unit 2c. The upward termination of fault f6 appears to be in unit 2b, and we could not trace any evidence of this fracture upward to the modern ground surface. Based on the mismatch in stratigraphic thicknesses and the juxtaposition of dissimilar units, we infer that this fault must have

significant lateral slip. The problem with a surface rupture interpretation at this stratigraphic level is that unit 2b apparently fills the depression left by event E3 and it is difficult to believe that the depression lasted for too long after the surface rupture. Thus, event E2 must have either occurred soon after event E3 or the site was closed to significant deposition for some extended period of time after event E3, which is possible considering the site's presence within the canal.

An alternative explanation is that fault f6 deformation is absorbed in the fine-grained fill of units 2b and 1 and that this fault was activated in 1999. Support for this idea is weak, but is based on the inference that unit 2b is only slightly younger in age than unit 2c, which appears to have directly resulted from the earlier event. However, the evidence for lateral slip along fault f6 is strong and would require a significant amount of strain being absorbed in unit 2b.

A third possibility is that unit 2c is a fluvial deposit that filled/eroded along the fault after event E3 and was faulted by both faults f6 and f7 during event E2. This possibility might be more attractive than the first explanation because it would permit more time between events E3 and E2. The fissuring of unit 2c downward into the fault could be explained by this mechanism and therefore would not require liquefaction of the sandy gravel of unit 2c.

We attribute event E3 to the large event of 1719 that had descriptions of damage that closely parallel those of 1999. It is the first large event after 1591 for this area and was apparently as large as 1999 (Ambraseys & Finkel 1995), consistent with the trench observations that indicate event E3 was a major surface rupture. Considering the case that event E2 occurred soon after E3, we attribute that deformation to either afterslip or possibly the 1754 earthquake, which is known to have produced damage in this region but for which the source is unknown. Later earthquakes, such as 1878 or 1894, appear to have occurred too long after event E3, and the surface soil of unit 1 would almost certainly have developed by that time.

The Köseköy site

The Köseköy site lies along a section of rupture in the SE corner of the township of Köseköy (Fig. 9), SE of Izmit and west of the end of the Ottoman canal. Rupture in this area in 1999 included about 2 m of slip along the primary fault strand, and secondary rupture along faults that splay off to the north from the main strand. The site is also in an area where the fault makes a small releasing stepover, and a strand to the south of our trench becomes the main strand farther east (Fig. 9).

Rockwell *et al.* (2002) report offsets of surveyed trees adjacent to this site to be on the order of 1.8–2.25 m, consistent with slip values reported from rupture mapping after the earthquake (Barka *et al.* 2002). To both the east and west of the Köseköy area, slip along the Izmit–Sapanca rupture segment generally exceeded 3 m in 1999, and slip values as high as 3.8 m based on surveyed data were reported by Rockwell *et al.* (2002). We interpret this to mean that slip is distributed across multiple strands in the Köseköy area. We chose this site in part because the secondary faulting could be demonstrated to be principally dip-slip, making recognition and reconstructions of past earthquakes easier. Furthermore, palaeoearthquakes are often more easily recognized where multiple fault splays are present, as some secondary faults may rupture in only one or two events. Finally, part of our group conducted radar profiles at this site and identified a buried palaeochannel that is apparently right-laterally offset about 6.6 m, roughly three times the 1999 slip (Ferry *et al.* 2004).

We excavated five trenches at this site (Fig. 9), with only trench T-3 crossing the main, northern strand of the fault. The active drainage generally runs parallel to the fault zone and lies immediately south of the end of trench 3 by about 2 m. Hence, we could not extend this trench to cross the southern main strand, which had lost most of its slip in this area. Trench T-1 was excavated across a purely dip-slip fault that experienced about 60 cm of slip in 1999. A nearby small berm and associated concrete flume displayed no evidence of lateral slip (Fig. 9), thereby confirming the normal slip inference for the fault in trench T-1. Thus, no out-of-plane transfer of sediments is expected in the sediments of trench T-1 and past events should be recognized by their dip separations.

The stratigraphy in trenches T-1 and T-3 is composed of a sequence of coarse- and fine-grained strata that are interpreted as fluvial channel and overbank deposits (Figs 11 and 12). We physically traced most units between trenches T-1 and T-3 via a connecting fault-parallel trench (trench T-2, not logged in detail). Most units display some degree of lateral variability, becoming slightly coarser or finer from one trench to the other. Nevertheless, we believe that the unit designations apply consistently for both trench exposures.

Unit 1 is a dark brown plough pan (topsoil A horizon) unit that was tilled frequently. Units 2 and 3 are bedded channel deposits, with unit 2 being a distinctive sandy gravel in trench T-1, grading to a massive cobbly gravel in trench T-3. Similarly, unit 3 is a stratified coarse- to fine-grained sand in trench T-1 that grades to cobbly gravel in trench T-3. These units pinch out to the north across a palaeoscarp in trench T-1 (Fig. 12) and locally
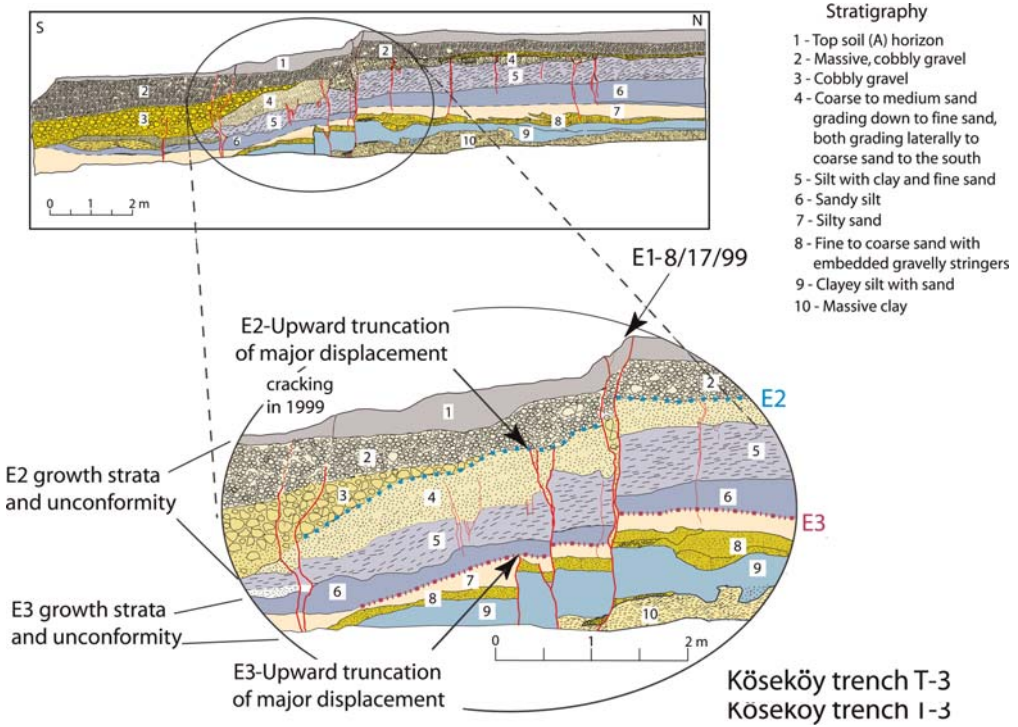
Fig. 11. Log of trench 3 at the Köseköy site. The 1999 Izmit surface rupture is indicated as E1, with two older ruptures interpreted as E2 and E3.
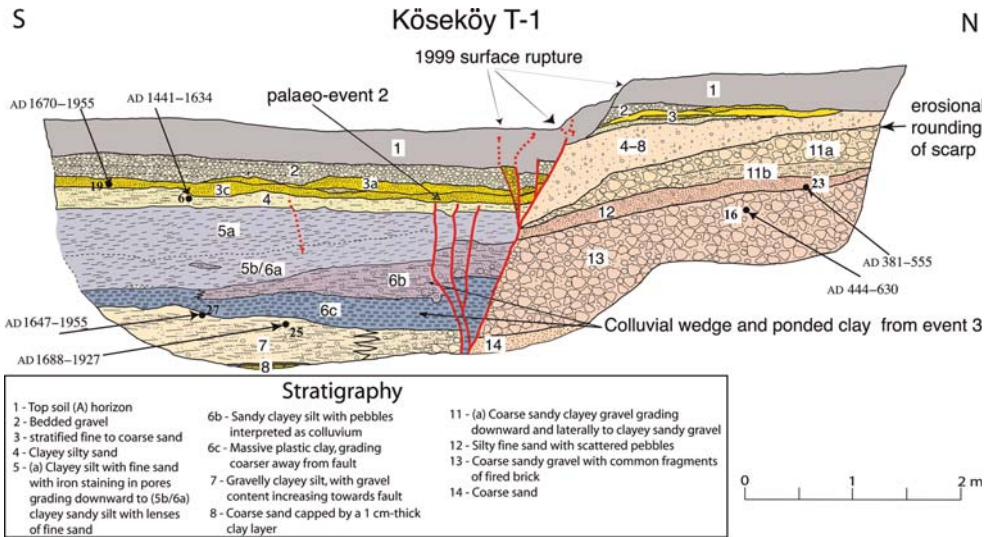

Fig. 12. Log of the Köseköy trench T-1. Unit designations stratigraphically match those given in Figure 11, hence there is no unit 9 or 10. Slip in 1999 was purely dip-slip, based on the lack of lateral offset of an adjacent flume and berm. Note the older fractures that did not rupture in 1999. Black dots with numbers are detrital charcoal sample locations for dates provided here and in Table 1.

scour into the underlying unit 4. We interpret this part of the section to represent a period of sedimentation prior to the current incision of a drainage located a few metres south of the southern end of trench T-3.

Unit 4 is a dark brown, massive, clayey silty sand (loam) that we interpret as a buried A horizon or topsoil in trench T-1, and this unit also coarsens towards the active drainage, becoming a coarse- to medium-grained sand in trench T-3. This unit was easily mappable south of the fault in T-1, but north of it, unit 4 appeared to become less distinct so we grouped it with underlying units as unit 4-8. Unit 5 is a weakly stratified clayey silt with sand that grades downward to a pebbly, sandy clayey silt. This unit is similar in all exposures and probably represents overbank sedimentation. North of the fault in trench T-1, the equivalent unit, unit 4-8 is a massive pebbly clayey silt that we interpret as predominantly of colluvial origin.

Unit 6 is a very distinctive plastic clay that was only exposed south of the fault in trench T-1 and appears to thicken towards the fault. We interpret the lower part of unit 6 as an overbank deposit, although it may be clay derived from overbank sedimentation ponded within the fault zone. The upper part of this unit thickens to the fault and may be a colluvial wedge shed from the scarp. Unit 6 coarsens southward to trench T-3, where it is of sandy silt composition.

Unit 7 is a gravelly clayey silt that appears very similar to unit 5 in trench T-1 but grades to a silty sand in trench T-3. In trench T-1, the gravel content is sparse away from the fault but increases towards the fault, suggesting a colluvial origin for part of this unit as well.

Finally, south of the fault in T-1, unit 8 is a distinctive coarse sand interpreted to be fluvial in origin. This sand was traced laterally towards trench T-3 and likely forms the channel deposit imaged by Ferry *et al.* (2004) in their radar survey. In trench T-3, the sand of unit 3 also contains stringers of fine gravel.

North of the fault, trench T-1 exposed several older units below unit 4–8. Unit 11 is a bedded coarse-grained sandy, clayey gravel interpreted to be of fluvial origin. There was no equivalent for this unit exposed south of the fault, although it is the probable source for the gravelly colluvium of unit 7. Unit 12 is a distinctive silty fine sand with scattered gravel, unit 13 is a coarsely bedded gravel containing abundant pottery and tile shards, and unit 14 is a distinctive coarse sand. Collectively, units 11 to 14 are interpreted as a fluvial sequence of strata preserved on the northern upthrown side of the fault zone.

Age control for the stratigraphy is provided by dating of individual detrital charcoal samples in trench T-1. Charcoal was abundant in our exposures, and we collected over 200 samples from the Köseköy site. In T-1 alone, nearly 40 samples were collected and we dated six. Four samples were dated from units 3 to 7 and two from the older units north of the fault.

All four samples from units 4–7 yielded modern or nearly modern results. The sample from unit 7 yielded a calibrated age of AD 1688–1927, requiring that all overlying units are also no older than 1688. Thus, most of the exposed section south of the fault was deposited during the past 335 years or so.

North of the fault, two samples were dated from units 10 and 11, with the lower sample from unit 11 yielding a calibrated date range of AD 444–630. As both sample ages are indistinguishable at 2σ, and as they both place the age of these units at about the fifth to sixth century AD, we accept these dates as the approximate age of this older fluvial section. Thus, there is a 1000-year-long hiatus in deposition on the northern side of the fault, although much of the record may be preserved at depth below the current base of T-1 to the south.

Interpretation of past earthquakes

We recognize evidence for three events recorded in the stratigraphy exposed in trenches T-1 and T-3. The most recent event is the August 1999 Izmit earthquake, and is designated as event E1. Earlier events are recognized in trench T-3 across the main fault by upward terminations of secondary splays and by tilting and growth strata. In trench T-1, earlier events are recognized on secondary splays and by the production of colluvial wedges that thin from the fault.

For instance, event E2 is indicated in the main zone by rupture of a fault splay up through unit 4, which is apparently capped by unit 2. However, unit 2 is gravel and it could be argued that slip on this fault strand is distributed in the gravel, so we rely more heavily on the dip-slip expressed from this event in trench T-1 (Fig. 13). There is apparently also tilting of units 4 and older below the inferred event E2 level in trench T-3, and there is a buttress unconformity and deposition of units 2 and 3 above this unconformity, all of which provide secondary evidence of event E2. In trench T-1, several secondary splays terminate upward at the top of unit 4, and units below this event horizon are thinner in the fault zone. This is especially evident in the reconstructions shown in Figure 13, where 1999 dip-slip was removed. In that the 1999 earthquake produced no lateral slip at trench T-1, we reconstruct the pre-1999 section assuming no out-of-plane motion (Fig. 13a), which required about 60 cm of dip reconstruction.
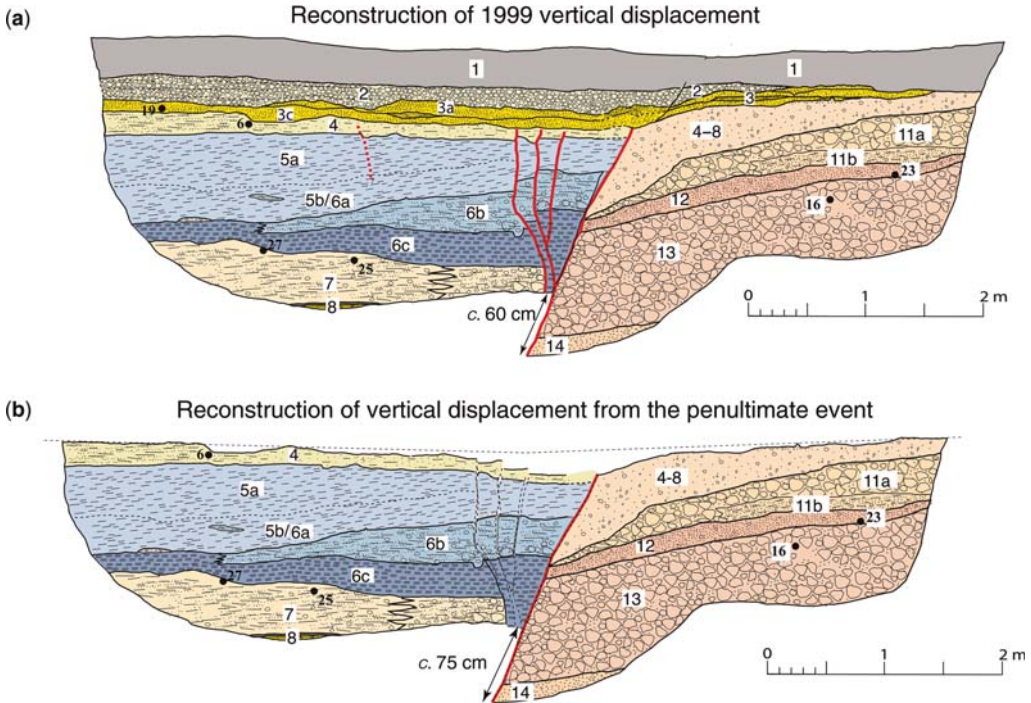
Fig. 13. Reconstruction of stratigraphy in trench T-1 to pre-1999 (**a**) and pre-penultimate event (**b**). Note the dip-slip was similar in each event. Refer to text for discussion of event interpretations.

In the log of trench T-1 in Figure 12, unit 3 pinches out north of the fault, indicating the presence of a scarp at that time. In the reconstruction of Figure 13a, these relationships are even more obvious, with units 2 and 3 pinching across a buried fault scarp produced by the penultimate event. Units 6 to 4 are faulted by the secondary strands and overlain by units 1–3. A degraded scarp that involves units 4 to 8 is also present. From these observations, we interpret event E2 to have occurred after the deposition of unit 4 and prior to the deposition of unit 3. Based on the ages of these units (Table 1), E2 must have occurred after AD 1688.

We attempted to remove the deformation of event E2 with further reconstruction of the units faulted in E2 (Fig. 13b). We reconstructed units 4 to 6 across the secondary strands, and restored or rematched units 4, 5 and 6 south of the fault to unit 4–8 north of it. This required an additional 15 cm of reconstruction, or about one-quarter of that required to remove the 1999 deformation. This reconstruction resulted in an apparent depression along the fault, part of which is explained by the uplift and subsequent erosion of unit 4 during and after event E2. The balance is explained

by erosion of unit 4–8 on the north after the formation of the scarp. The volume of soil represented by this depression was evidently removed by erosion and subsequent deposition of the unit 3 channel deposits.

With the reconstruction shown in Figure 13b, we observe that unit 6c fills a depression in the fault zone (fissure fill?) that is capped by unit 6b. Unit 6b itself has a wedge-shaped geometry that we interpret as a colluvial wedge shed from the fault scarp. Based on this interpretation, event E3 occurred during deposition of unit 6. The amount of vertical slip for event E3 is similar to or more than that of 1999 if units 6b and 6c are deposited against the scarp formed in that event (the wedge thickness at the fault would be less than the actual amount of dip-slip during the causative earthquake).

There is also direct evidence for event E3 in trench T-3 across the main fault zone. Two fault splays about 1 m south of the main 1999 break rupture up through unit 7 and the base of unit 6, and are capped by additional unit 6 deposits. A radiocarbon sample recovered from unit 7 in trench T-1 post-dates AD 1688, indicating that all three of the recognized events occurred in the past 320 years.

Another observation that is consistent with the occurrence of three events after deposition of unit 8 is based on a radar survey conducted by Ferry *et al.* (2004). Prior to the trenching, they ran radar surveys parallel to the 1999 rupture and imaged a buried channel on each side of the fault. North of the main rupture, we encountered this channel in our trench 2. South of the fault, the interpreted correlative channel is laterally displaced about 6.7–7.4 m westward. We attempted to trench to the depth of the channel on the south side of the fault. However, saturated conditions and a collapsing trench wall precluded a direct look at this deposit south of the fault. If the radar correlation and estimate of slip is valid, approximately three times the amount of 1999 slip as occurred on the main rupture would be required to restore the lateral offset of the unit 8 channel. This is consistent with our inference that three events are required to explain all of the relationships observed in trench T-1, although not all were necessarily the same size.

Event E1 is the 1999 Izmit rupture. Events E2 and E3 must post-date 1688, and one is almost certainly the large 1719 earthquake that had a very similar damage distribution to 1999 (Ambraseys & Finkel 1995). Considering that 1719 is only a few decades after the bounding radiocarbon control, it is most likely that E3 corresponds to the 1719 surface rupture.

Our observations also suggest that vertical slip on the secondary normal fault in event E2 was smaller than that of 1999, although this may not reflect the amount of lateral displacement on the main fault. It is also possible that this secondary fault displays variable amounts of slip in each earthquake, possibly as a consequence of rupture direction. In any case, it is possible that event E2 was smaller than 1719 or 1999, and is possibly either 1754, 1878 or 1894. The 1754 source zone is not well known but is reported to have produced more damage in Istanbul (Ambraseys & Finkel 1995) than that which occurred in 1999. Damage from 1719 was reported from Istanbul to Bolu, whereas damage in 1754 was more strongly focused to the west. From those observations, 1754 was either larger or farther west than 1999. If the main shock of 1754 was in the Gulf of Izmit, as suggested by Ambraseys & Finkel (1991, 1995), then it is also possible that some slip propagated onto the Izmit–Sapanca segment that had ruptured only a few decades earlier. The 1878 event, in contrast, is believed to have occurred farther east than 1754 based on damage reports, but there is also much less known. Ambraseys & Finkel (1991) and Ambraseys (2000) report this as a locally destructive event between Eşme, Sapanca and Adapazarı, with damage extending to Akyazı, Izmit and Bursa. Taken at face value, the damage zone is

considerably smaller than 1719 or 1754, although an east-directed rupture of smaller magnitude may be consistent with the 1878 damage effects. However, the damage zone for 1878 may be too small to be consistent with a major surface-rupturing event. In the final analysis, more historical reports on damage are needed to determine whether 1878 is a viable candidate earthquake for event E2.

The M7.3 1894 earthquake is also suggested to have ruptured from Sapanca to Izmit Bay based on historical reports of damage (Ambraseys 2001), and this earthquake would likely have resulted in surface rupture at both the Ottoman Canal and Köseköy sites if it indeed ruptured east of Izmit. (Klinger *et al.* 2003 did not see evidence for this event at their Gölcük trench site, however.) Ambraseys (2001) reports this as a large earthquake that was only slightly smaller than 1999. If correct, and if event E2 corresponds to this earthquake, then the observed smaller vertical displacement associated with E2 on the secondary strand probably reflects inherent variability in vertical displacement associated with secondary faults. Thus, there are three plausible candidates for event E2 between Izmit and Sapanca, with the potential size ranging from relatively small (1878) to relatively large (1894).

The record is too short to develop a meaningful slip rate at the Köseköy site. Nevertheless, the return period for large earthquakes in the past 350 years appears to be in the range of 140 years (1719, 1754 or 1878 or 1894, and 1999). However, based on the amount of displacement on the secondary fault exposed in T-1 at Köseköy, it is not clear if all events have similar displacement at the Köseköy trench site. In 1999, slip across the entire fault zone near our Köseköy trench site was measured from offset tree lines at *c.* 3–3.8 m (Rockwell *et al.* 2002), although we only measured about 2 m on the main strand at trench T-3. If Ferry *et al.* (2004) have correctly defined lateral displacement for all three events, then each may have been large in the Köseköy area and a rate as high as *c.* 24 mm/a is estimated, which is close to the GPS rate of 24 ± 1 mm/a (McClusky *et al.* 2000) to 28 ± 0.3 mm/a (Reilinger *et al.* 2006). Alternatively, if some events are smaller, such as suggested by the vertical component of event E2, then this likely represents a maximum rate for the past several hundred years.

Discussion of results

There are three primary conclusions from our work. First, it appears that 7–9 m of slip has accrued on the NAF both east and west of the Marmara Sea in the past 300 years. During this period, only the

April 1766 earthquake has released significant stored strain in the central Marmara itself (Ambraseys & Jackson 2000), leading to the conclusion that the Marmara is ripe for a large earthquake, consistent with interpretations by Parsons *et al.* (2000). Armijo *et al.* (2005) suggest that the 1912 earthquake may have ruptured well eastward into the Marmara based on the freshness of scarps on the sea floor. However, it is not clear how long such scarps can be preserved at the bottom of these deep basins and some of these may have survived since 1766. Further, the isoseisms for 1912 are much stronger to the west, with less damage at Tekirdag (Fig. 1) than farther west. Damage observations argue that either the 1912 rupture terminated well before the central Marmara or that the rupture propagated westward, resulting in substantial directivity of energy and concentration of damage on the Gallipoli peninsula. In either case, the central Marmara segment closest to Istanbul has apparently not failed since 1766 (or possibly 1509; Ambraseys & Jackson 2000), so hazard is high when the behaviour of adjacent segments is considered.

A second general observation is that the NAF slip rate over the past millennium is apparently lower than that indicated by GPS west of the Marmara Sea. At Saros, we determined a return period of about 283 ± 113 years, which, when combined with average displacement for the past two surface ruptures (and assuming that this average displacement is applicable for earlier events), yields a millennial rate of *c.* 16 mm/a. Relienger *et al.* (2006) interpret GPS data to represent 26–28 mm/a of loading in the Gallipoli peninsular region, which is considerably higher than what has apparently been released in the past thousand years or so. There are three obvious explanations for this apparent discrepancy. First, it is likely that we do not record the full amount of displacement in our trenches. We determined 3D slip at only one site whereas slip can vary substantially along a rupture, as demonstrated by Rockwell *et al.* (2002) for the 1999 Izmit earthquake. In their study, they found an average of 15% distributed near-field deformation represented by warping into the fault. As this deformation extends out for several metres in areas of deep alluvium, and such is likely the case for the Saros study site, we may have determined only the minimum average displacement for the 1912 and 1766 earthquakes. Further, slip varies laterally along a rupture by 20% or more over relatively short distances, so we may have trenched in a low slip area. However, to increase displacement to that required to satisfy the GPS rate would require that the average displacement per event increase to about 6.7 m. Although this is possible, Altunel *et al.* (2004) suggest that

the average far-field value for the 1912 surface rupture is closer to 4–5 m, consistent with our trench results.

For a similar length of record, Klinger *et al.* (2003) studied the rupture history of the NAF at Gölcük, where they determined that the fault had ruptured only three times since the fifteenth century. They attributed the surface ruptures described in their trenches to the large events of 1509, 1719 and 1999, which suggests a return period for large earthquakes for that segment of the NAF of about 250 years. Maximum slip at Gölcük in 1999 was about 4.5–5 m (Barka *et al.* 2002), which when combined with the return period, suggests a short-term rate of 18–20 mm/a. Farther east, along the 1944 rupture, Okumura *et al.* (2004), Rockwell *et al.* (2004) and Kondo *et al.* (2004) have determined about 25 m of slip for the past 1500 years, which also yields a rate of *c.* 16 mm/a. In summary, the NAF appears to have a surface slip rate for the past 500–1200 years, and possibly longer, that is significantly lower than that interpreted from GPS data, and this observation appears to be true both east and west of the Marmara Sea. It is possible that the past 1000 to 1500 years is too short an interval to assess the rate, and that strain release is variable over the several-thousand-year timeframe. In this scenario, the past thousand years have simply seen a relative lull in seismic slip. Alternatively, the GPS rate may be too high, at least in terms of slip on the main NAF. This can be explained by either a lower long-term GPS rate with the current observations affected by the >1000 km sequence of ruptures this past century, or by more broadly distributed slip across the NAF zone, with secondary faults accommodating up to 20% of the deformation.

A third conclusion from our trench study between Izmit and Sapanca is that this segment apparently ruptures more frequently than the section to the west (Klinger *et al.* 2003). Slip in 1999 was lower, averaging about 3–3.5 m near Izmit versus 4–5 m to the east and west (Barka *et al.* 2002). This *c.* 30-km-long segment is bound by relatively small step-overs at Lake Sapanca (1–2 km) and Gölcük (1–2 km) (Lettis *et al.* 2002), and thus appears to be weaker than the adjacent sections and can apparently fail on its own as indicated by the shorter return period and smaller amount of slip inferred for event E2. If E2 was, in fact, the result of the 1754 rupture, then it appears that re-rupture of this segment can occur after only a few decades. This is contrary to the general idea that the Izmit to Sapanca area is safe from a near-future rupture because it just sustained slip in 1999. In contrast, if E2 was 1878 or 1894, then the Izmit–Sapanca segment appears to have more periodic behaviour. Future work along this segment should concentrate

on better dating of the penultimate rupture, as there are clear implications for future hazard and rupture behaviour.

References

ALTINOK, Y., ALPAR, B. & YALTIRAK, C. 2003. Şarköy–Mürefte 1912 Earthquake's Tsunami, extension of the associated faulting in the Marmara Sea, Turkey. *Journal of Seismology*, **7**(3), 329–346.

ALTUNEL, E., MEGHRAOUI, M., AKYUZ, S. & DIKBAS, A. 2004. Characteristics of the 1912 co-seismic rupture along the North Anatolian Fault Zone (Turkey): Implications for the expected Marmara earthquake. *Terra Nova*, **16**(4), 198–204.

AMBRASEYS, N. N. 2000. The seismicity of the Marmara Sea area, 1800–1899. *Journal of Earthquake Engineering*, **4**(3), 377–401.

AMBRASEYS, N. 2001. The earthquake of 10 July 1894 in the Gulf of Izmit (Turkey) and its relation to the earthquake of 17 August 1999. *Journal of Seismology*, **5**, 117–128.

AMBRASEYS, N. N. 2002*a*. The seismic activity of the Marmara Sea region over the last 2000 years. *Bulletin of Seismological Society of America*, **92**(1), 1–18.

AMBRASEYS, N. N. 2002*b*. Seismic sea-waves in the Marmara Sea region during the last 20 centuries. *Journal of Seismology*, **6**(4), 571–578.

AMBRASEYS, N. N. & FINKEL, C. F. 1987*a*. The Saros-Marmara earthquake of 9 August, 1912. *Earthquake Engineering and Structural Dynamics*, **15**, 189–211.

AMBRASEYS, N. N. & FINKEL, C. F. 1987*b*. Seismicity of Turkey and neighboring regions, 1899–1915. *Annales Geophysicae*, **5B**, 701–726.

AMBRASEYS, N. N. & FINKEL, C. F. 1991. Long-term seismicity of Istanbul and the Marmara Sea region. *Terra Nova*, **3**, 527–539.

AMBRASEYS, N. N. & FINKEL, C. F. 1995. *The Seismicity of Turkey and Adjacent Areas, A Historical Review, 1500–1800*. Eren Yayıncılık, Istanbul.

AMBRASEYS, N. N. & JACKSON, J. A. 2000. Seismicity of the Sea of Marmara (Turkey) since 1500. *Geophysical Journal International*, **141**, F1–F6.

ARMIJO, R., PONDARD, N. *ET AL.* 2005. Submarine fault scarps in the Sea of Marmara pull-apart (North Anatolian Fault): Implications for seismic hazard in Istanbul. *Geochemistry, Geophysics, Geosystems*, **6**, 1–29.

BARKA, A. A. 1992. The North Anatolian fault zone. *Annales Tectonicae*, **6**, 164–195.

BARKA, A., AKYUZ, H. S. *ET AL.* 2002. The surface rupture and slip distribution of the 17 August 1999 Izmit earthquake (M7.4), North Anatolian fault. *Bulletin of the Seismological Society of America* (Special Issue on the 1999 Izmit and Düzce, Turkey, Earthquakes, N. Toksoz (ed.)), **92**(1), 43–60.

BRONK RAMSEY, C. 2005. OxCal Program v3.10. www.rlaha.ox.ac.uk/oxcal/oxcal.htm.

FERRY, M., MEGHRAOUI, M., GIRAD, J.-F., ROCKWELL, T. K., KOZACI, A., AKYUZ, S. & BARKA, A. 2004. Ground-penetrating radar investigations along the North Anatolian fault near Izmit, Turkey: Constraints on the right-lateral movement and slip history. *Geology*, **32**(1), 85–88.

FINKEL, C. & BARKA, A. 1997. The Sakarya River-Lake Sapanca-Izmit Bay canal project: A reappraisal of the historical record in the light of new morphological evidence. *Istanbuler Mitteilungen*, **47**, 429–442.

KLINGER, Y., SIEH, K. *ET AL.* 2003. Paleoseismic evidence of characteristic slip on the western segment of the North Anatolian fault, Turkey. *Bulletin of the Seismological Society of America*, **93**(6), 2317–2332.

KONDO, H., OZAKSOY, V., YILDIRIM, C., AWATA, Y., EMRE, O. & OKUMURA, K. 2004. 3D trenching survey at Demir Tepe site on the 1944 earthquake rupture, North Anatolian fault system, Turkey. *Annual Report on Active Fault and Paleoearthquake Research*, **4**, 231–242.

LETTIS, W., BACHHUBER, J., WITTER, R., BRANKMAN, C., RANDOLPH, C. E., BARKA, A., PAGE, W. D. & KAYA, A. 2002. Influence of releasing step-overs on surface rupture and fault segmentation: Examples from the 17 August 1999 Izmit earthquake on the North Anatolian fault, Turkey. *Bulletin of the Seismological Society of America*, **92**(1), 19–42.

MCCLUSKY, S., BALASSANIAN, S. *ET AL.* 2000. Global positioning system constraints on plate kinematics and dynamics in the eastern Mediterranean and Caucasus. *Journal of Geophysical Research*, **105**, 5695–5719.

OKUMURA, K., KONDO, H. *ET AL.* 2004. *Slip history of the 1944 Segment of the North Anatolian Fault to Quantify Irregularity of the Recurrence*. Geological Society of America Annual Meeting, **04-103**.

PARSONS, T., TODA, S., STEIN, R., BARKA, A. & DIETRICH, J. H. 2000. Heightened odds of large earthquakes near Istanbul: An interaction-based probability calculation. *Science*, **288**, 661–665.

RAMSEY, C. B. 2000. *OxCal Program Ver. 3.5*. Radiocarbon Accelerator Unit, University of Oxford. Available at: http://units.ox.ac.uk/departments/rlaha/orau/06_01.htm

REILINGER, R. E., MCCKUSKY, S. C. *ET AL.* 1997. Global positioning system measurements of present-day crustal movements in the Arabian-African-Eurasian plate collision zone. *Journal of Geophysical Research*, **102**, 9983–9999.

REILINGER, R., MCCLUSKY, S., VERNANT, P. *ET AL.* 2006. GPS constraints on continental deformation in the Africa-Arabia-Eurasia continental collision zone and implications for the dynamics of plate interactions. *Journal of Geophysical Research*, **111**, B05411, doi:10.1029/2005JB004051.

REIMER, P. J., BAILLIE, M. G. L., BARD, E. *ET AL*. 2004. IntCal04 Terrestrial Radiocarbon Age Calibration, 0–26 cal kyr BP. *Radiocarbon*, **46**, 1029–1058.

ROCKWELL, T., BARKA, A., DAWSON, T., THORUP, K. & AKYUZ, S. 2001. Paleoseismology of the Gazıköy-Saros segment of the North Anatolia fault, northwestern Turkey: Comparison of the historical and paleoseismic records, implications of regional seismic hazard, and models of earthquake recurrence. *Journal of Seismology*, **5**(3), 433–448.

ROCKWELL, T. K., LINDVALL, S., DAWSON, T., LANGRIDGE, R., LETTIS, W. & KLINGER, Y. 2002. Lateral offsets on surveyed cultural features resulting from the 1999 Izmit and Düzce earthquakes, Turkey. *Bulletin of the Seismological Society of America*, **92**(1), 79–94.

ROCKWELL, T. K., OKUMURA, K. *ET AL*. 2004. Paleoseismology of the 1912, 1944 and 1999 ruptures on the North Anatolian Fault: implications for long-term patterns of strain release. *Geological Society of America, Abstracts with Programs*, **36**(5), 51.

SIEH, K. 1996. The repetition of large-earthquake ruptures. *Proceedings of the National Academy of Sciences*, **93**, 3764–3771.

STRAUB, C. & KAHLE, H. 1995. Active crustal deformation in the Marmara Sea region, NW Anatolia, inferred from GPS measurements. *Geophysical Research Letters*, **22**(18), 2533–2536.

STRAUB, C. S. 1996. *Recent crustal deformation and strain accumulation in the Marmara Sea region, N.W. Anatolia, inferred from GPS measurements*. PhD dissertation, Swiss Federal Institute of Technology at Zurich.